HIGH-ENTHALY CHARACTERIZATION OF THE UTA HYPERSONIC SHOCK TUNNEL

by

RAHEEM TEMITOPE BELLO

Presented to the Faculty of the Graduate School of
The University of Texas at Arlington in Partial Fulfillment
of the Requirements
for the Degree of

MASTER OF SCIENCE IN AEROSPACE ENGINEERING

THE UNIVERSITY OF TEXAS AT ARLINGTON
December 2012

Dedicated to Nusirat Afinnih

ACKNOWLEDGEMENTS

First of all, I would like to thank Dr. Donald Wilson and Dr. Frank Lu for their guidance, patience, kindness, and the opportunity to work at the Aerodynamic Research Center. I am grateful to everyone for welcoming my questions and for the friendly atmosphere at the ARC.

I greatly appreciate the technical staff of the Mechanical and Aerospace Department, who helped make this work possible. Special thanks to the late Rod Duke for his invaluable help in making tunnel modifications. I would also like to thank Kermit Beird and Sam Williams in the Woolf Hall Machine Shop. Thanks also to David Carter, who ensured that the experiments were conducted safely.

I wish to thank my fellow Hypersonic Tunnel team mates, who graciously gave me assistance on my project as I prepared the runs. I particularly wish to thank Tiago Rolim, for making time to answer my questions and helping with the various experimental aspects of my project. Thanks also to Nitesh Manjunatha, Dibesh Joshi, Eric Braun, Pravin Vadassery, and Derek Leamon.

Lastly, I would like to thank my friends and family; my parents for being so supportive and encouraging in all my endeavors, and my brothers for always keeping me grounded.

November 26, 2012

ABSTRACT

HIGH-ENTHALPY CHARACTERIZATION OF THE UTA

HYPERSONIC SHOCK TUNNEL

Raheem Temitope Bello, M.S.

The University of Texas at Arlington, 2012

Supervising Professor: Donald R. Wilson

In hypersonic wind tunnel testing, matching the flow enthalpy conditions for the hypersonic air-breathing corridor is of great importance in order to assure the validity of experimental results. The flow enthalpy of the UTA hypersonic shock tunnel is increased by a shock-induced detonation driver. The detonation mixture consist of hydrogen and oxygen in stoichiometric quantities ($2H_2+O_2 \rightarrow 2H_2O$). Experimental variations of pressure and the volume of the detonation section were performed to characterize the enthalpy limits, and overall performance of the UTA hypersonic shock tunnel. The UTA HST test section was operated at a nominal Mach number of 10. Force balance experiments were performed in the test section during the high enthalpy characterization. Enthalpy measurements were also performed using a type K thermocouple placed in a Fay-Riddell probe within the test section. High enthalpy flows with maximum total temperature of 4393 K, maximum total pressure of 373 atm, and maximum total enthalpy of 5.1 MJ/kg were achieved in the driven section, with Mach numbers of 8.75 $\pm$ 0.25 measured in the test section.

TABLE OF CONTENTS

LIST OF ILLUSTRATIONS

Figure Page

LIST OF TABLES

NOMENCLATURE

a	speed of sound
h	enthalpy
M	Mach number
p	pressure
R	universal gas constant
T	temperature
u	velocity
γ	Specific heat ratio
ρ	density

Subscript

Pit	pitot
Ref	reference condition
t	stagnation condition
0	ambient conditions
1	initial driven section condition
100	initial detonation section condition
4	initial driver condition
5	condition behind reflected shock

Superscript

^{o}	degree
*	sonic condition

CHAPTER 1

INTRODUCTION

The use of hypersonic shock tunnels for aerodynamic research is critical in the understanding of the conditions present in hypersonic flight. In the development of hypersonic vehicles, testing of components such as scramjets and vehicle models in shock tunnels are essential for successful flights. Shock tunnel testing can provide information on engine performance, and measurements of drag and lift can be used to characterize aerodynamic performance of flight vehicles. The primary challenges of hypersonic shock tunnels are short steady test times, and creating uniform flows which match desired Mach number, and enthalpy conditions.

1.1 Literature Survey

Hypersonic shock tunnels have been in development since the 1950's, and have been further developed by Warren and Harris in the 1970's [1]. Impulse facilities such as shock tunnels have short test times ranging from micro-seconds to a few hundred milliseconds, and can be operated in reflected or non-reflected driven modes [2]. Impulse facilities operate by the abrupt discharge of a highly compressed gas, contained in a driver section into a region of lower pressure through the rupturing of a diaphragm. The upstream and downstream detonation driver modes were first investigated by Bird in 1957 [3].

1.2 Objective

The performance of the UTA hypersonic tunnel was previously characterized for low enthalpy flows [4]. The flow conditions created by the wind tunnel in low-enthalpy runs simulate perfect gas conditions at Mach 10. The present research focuses on characterizing the overall performance of the UTA hypersonic shock tunnel and creating high-enthalpy flow conditions,

matching Mach 10 flight in the hypersonic air-breathing corridor, hence accounting for real gas effects.

This research concentrates on the development of a shock-induced detonation driver to increase the enthalpy of the UTA hypersonic shock tunnel. Two sets of test section experiments were conducted during the calibration studies. These include measurements of aerodynamic drag using a force balance detailed in Chapter 2. Heat flux measurements performed in the test section were conducted using a type K (Chromel-Alumel) thermocouple, in a rake detailed in Chapter 2.

The detonation driver is accomplished by igniting an oxy-hydrogen mixture with a strong shock wave. The performance of the detonation driver is characterized by pressure measurements along the detonation section, driver section and in the test section. Using nine PCB 111A23 pressure transducers mounted on the detonation and driven tubes, the detonation and shock velocities were measured using the time-of-flight method [5]. The test section models were mounted with PCB 111A24 pressure transducers positioned in the core flow of the nozzle. The test section transducers measure the pitot pressure of the expanded flow, and are essential in the calculation of the test section Mach number.

1.3 Theory of Operation

A typical hypersonic shock tunnel consists of a shock tube, nozzle, test section, diffuser, and vacuum tank. The shock tube includes a driver section filled with high pressure gas, separated by airtight diaphragms from a driven tube which contains the low pressure test gas. The divergent nozzle attached to the shock tube expands the flow to hypersonic Mach numbers into the test section, where an experimental model is mounted. The diffuser reduces the flow Mach number by a converging section. The diffuser then empties the flow into the vacuum tank. A detonation section is incorporated between the driver section and the driven tube in a detonation driven shock tube.

The detonation-driven shock tunnel may be operated in a downstream or upstream mode. In the downstream or forward propagating mode, the detonation wave is shock induced. The wave initiation source is downstream of the driver, and results in an expansion wave in the driver and an incident shock wave in the detonation section. The shockwave ignites the combustible mixture, and following a deflagration to detonation transition, the resultant detonation wave's high pressure ruptures the diaphragm and initiates an incident shock wave in the driven tube. The repeatability of a shock-induced detonation-driven shock tunnel is excellent, as it is primarily dependent on the innate ability to control the diaphragm rupture.

In the upstream or backward propagating mode, the detonation wave is triggered by an electric arc. The detonation wave travels upstream, and is reflected off the closed end of the driver, generating very high pressures. The reflected detonation wave then travels downstream, ruptures the diaphragm and initiates an incident shock wave in the driven tube. Precaution should be taken to ensure that the high pressures created by reflection of the detonation wave do not exceed the structural limits of the driver. A damping tube may be used ensure that the structural integrity of the driver is not compromised.

The upstream mode results in a more uniform flow, although at a lower enthalpy, in contrast to the downstream mode with equivalent initial conditions. The gas momentum in the downstream mode yields better performance in contrast to the upstream mode where the energy from the initial gas momentum is significantly reduced due to the reflection. However, in the downstream mode, Taylor rarefactions behind the incident detonation wave results in a non-uniform detonation driver gas flow, yielding a reduced test time in the test section.

In the upstream detonation-driven shock tunnel, the shock may induce an under-driven, perfectly-driven, or over-driven detonation wave. The under-driven mode occurs when the pressure behind the incident shock wave of the driver gas is less than the Chapman-Jouguet pressure of the detonation wave ($p_{400} < p_{CJ}$). Taylor rarefactions following the detonation wave are present in the under-driven mode, and can be eliminated in the perfectly-driven mode.

In the perfectly-driven mode, the pressure of the driver gas behind the incident shockwave balances the Chapman-Jouguet pressure of the detonation wave ($P_{400} = P_{CJ}$). Any further increase in the initial driver gas pressure p_4, will result in the expanded driver gas being higher than the Chapman-Jouguet pressure of the detonation wave ($P_{400} > P_{CJ}$), creating the over-driven condition. Therefore the detonation wave will travel faster than the Chapman-Jouguet detonation velocity. The shock-induced detonation driver may approach the perfectly-driven mode, when a light gas such as helium or hydrogen is used as the driver gas, the initial pressure and temperature are high in the driver, the post detonation pressure is low, and the Chapman-Jouguet detonation wave velocity is small.

1.3.1 Shock Tunnels

Shock tubes consist of a driver with high-pressure gases, and a low-pressure driven tube separated by an airtight diaphragm. The performance of shock tubes is limited to supersonic Mach numbers. Abraham Hertzberg proposed the addition of a divergent nozzle to a shock tube to expand flows from a shock tube to hypersonic numbers [6]. Shock tubes with a divergent nozzle attached are referred to as shock tunnels.

A shock tunnel may be designed as a non-reflected or reflected one. A non-reflected shock tunnel expands the flow directly from the shock tube [Figure 1.1]. The minimum area of the divergent nozzle is equal to the area of the shock tube's exit. The incident shock wave travels directly into the nozzle. The total pressure is limited to the pressure behind the incident shock wave. The boundary layers in non-reflected shock tunnels are large. The boundary layers in the shock tube are transmitted into the nozzle, which intensifies the boundary layer growth. Therefore methods may be implemented to reduce boundary layer growth. The uniform flow is behind the incident shock wave and is terminated by the contact surface. Figure 1.1 shows a schematic for a non-reflected shock tunnel.

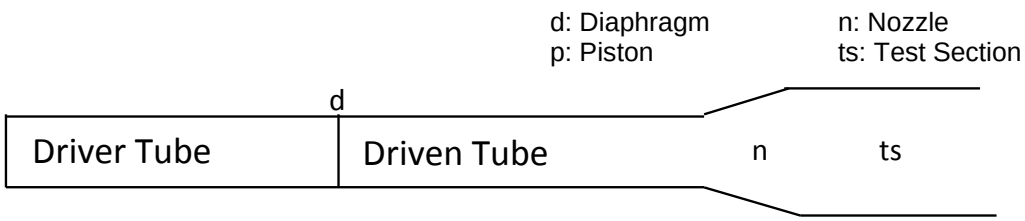

Figure 1.1 Schematic for a non-reflected shock tunnel

A reflected shock tunnel uses a secondary diaphragm between the shock tube and the divergent nozzle, to reflect the incident shock wave [Figure 1.2]. The sections downstream of the secondary diaphragm are evacuated to a low pressure to ensure that the tunnel starts and to yield an adequate test time. The reflected shock increases the stagnation pressure, allowing the flow to be expanded to higher Mach numbers in contrast to a non-reflected tunnel. The high pressure created by the reflected incident shock ruptures the secondary diaphragm, initiating the flow through the nozzle.

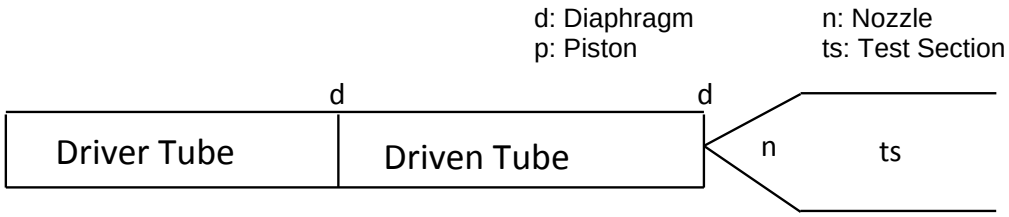

Figure 1.2 Schematic for a reflected shock tunnel

1.3.2 Shock Tunnel Improvement Techniques

There are several methods used to improve the performance of shock tunnels. These techniques include the light gas driver, the high temperature driver, the free-piston driver, and the detonation driver.

The light-gas driver requires that the driver section is filled with a light gas such as helium. The high-temperature driver requires that the gas temperature of the driver section is increased using a heater. These two techniques improve performance over a cold air driver, by aiming to increase the sound speed of the driver gas. For the light-gas driver, helium has a lower molecular weight than air which is mostly nitrogen, hence has a higher speed of sound

than air. In the high-temperature driver, the increase in the speed of sound is a function of the square-root of temperature $a \sim T^{0.5}$. The higher speed of sound results in higher incident shock Mach numbers, for similar driver-to-driven tube section pressure ratio p_4/p_1 of a simple cold air driver.

The free-piston driver was first proposed by Stalker in 1967 [7], and has been used to achieve the highest enthalpy flows in shock tunnels [Figure 1.3]. This technique involves compressing the driver gas by a heavy piston. The piston is accelerated to very high speeds, by high pressure air in the reservoir. The driven gas is compressed by the piston to achieve the desired test pressures and temperature. The operation of a free piston driver is complex, as it requires a rapid acceleration and deceleration of a heavy piston from near supersonic speeds in an orderly way.

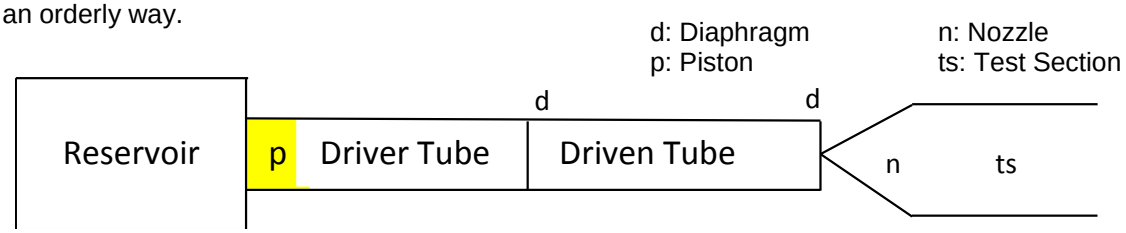

Figure 1.3 Schematic for a free-piston driven shock tunnel

The detonation driver is a simpler approach used to improve the performance of shock tunnels, researched by Bird [3] in 1957 [Figure 1.4]. The detonation driver acts like a gaseous piston driver, using detonation mixtures such as oxy-hydrogen mixtures. The detonation wave transitions into a shockwave which compresses the driven gas to desired pressures and temperatures. The enthalpies achieved by a detonation driver are lower than a free-piston driver, but extremely high enthalpies can still be achieved using a detonation driver. The pre-detonation pressure of the gaseous mixture is usually only a few atmospheres, but the post-detonation pressure increases by a factor of ~20 for an oxy-hydrogen mixture. The limitation of a detonation driver is therefore based on preserving the structural integrity of the shock tunnel to withstand the sudden and short duration high pressure and temperature increase due to the detonation wave.

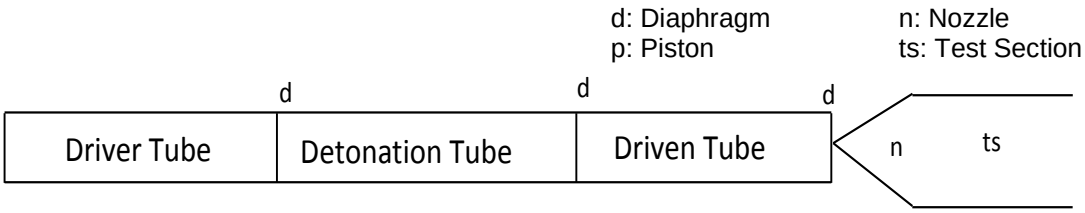

Figure 1.4 Schematic for a detonation driven shock tunnel

Another proposed shock tunnel improvement technique [5] involves the combination of a detonation driver and a free piston driver to maximize the performance of a shock tunnel [Figure 1.5]. This resultant enthalpy of this tunnel configuration can be computed by superposing the outcomes of both the detonation-driven and free-piston tunnel, although the challenges of operation make this configuration arduous.

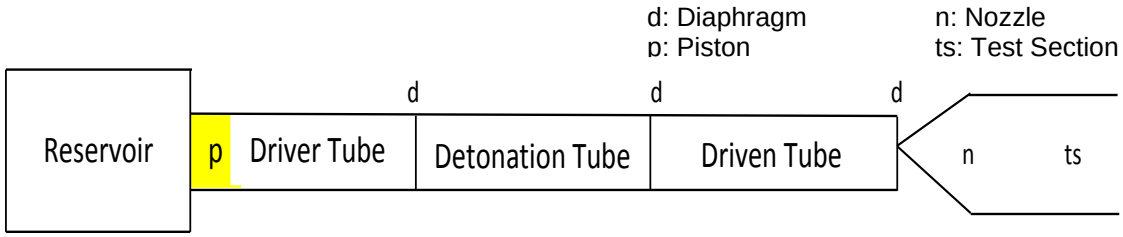

Figure 1.5 Schematic for a free-piston detonation driven shock tunnel

.

CHAPTER 2

INTRODUCTION

2.1 Tunnel Description

The UTA Aerodynamics Research Center hypersonic shock tunnel is a reflected shock tunnel [8]. The tunnel's main components includes a driver section tube, diaphragm section, driven tubes, nozzle, test section, diffuser, and dump tank, shown in Figure 2.4. A detonation section is included between the diaphragm and driven tube sections in the high-enthalpy configuration.

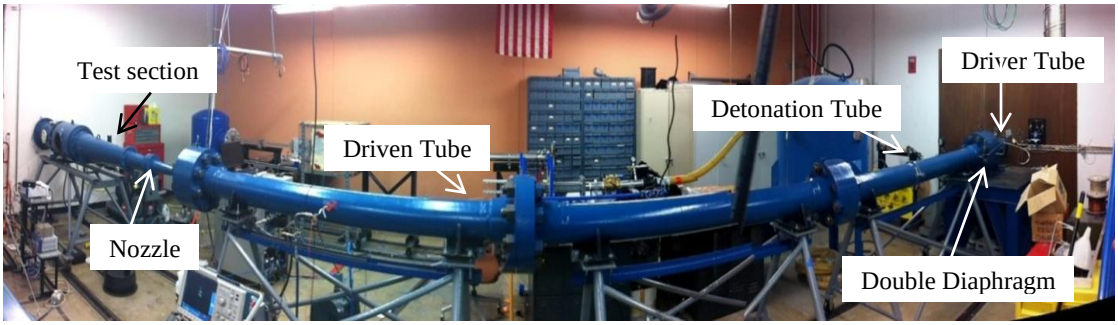

Figure 2.1 Panoramic picture of the UTA hypersonic shock tunnel; adapted from Vadassery [9].

The driver tube stores the high-pressure driver gas (air or helium). It is a lone section fabricated from steel, and is rated for a maximum operating pressure of 6000 psi. The tube is 10 ft in length, has an internal diameter of 6 inch, and a wall thickness of 1 inch. The driver tube has one end closed off with a hemispherical cap. The open end has a welded flange 4.5 inches thick and 19 inches in diameter. This flange connects the driver section to the diaphragm section, by eight 18 inch long and 2 inch diameter steel bolts.

The diaphragm section separates the high-pressure gas in the driver section from the low-pressure detonation or driven tube. Two diaphragms are placed in the diaphragm section, in order to create a controlled rupture pressure difference using the double diaphragm technique.

The diaphragm section consists of three flanges, two of which are attached to the driver and driven tube each and a third flange in between, freely supported by the eight steel bolts which connect the sections. The middle flange has four steel rods which support the two diaphragms. The flanges all have the same dimensions described earlier, and have O-ring grooves machined in them to ensure a tight seal.

The driven section stores the low-pressure test gas. It is comprised of three steel tubes 9 ft in length, with internal diameters of 6 inch. The tubes are rated for a maximum pressure of 6000 psi. The three tube segments are connected by flanges, with similar dimensions as the driver section, by 2 inch diameter steel bolts. The faces of the driver section flanges protrude by 0.5 inch and lock into the next tube section, which is counter bored by 0.5 inch.

The detonation section stores the detonable mixture such as an oxy-hydrogen mixture. The detonation section comprises of one or two driven section tubes following the double diaphragm section. The depressed section in the driver tube is critical in placing a 0.01 inch Mylar diaphragm to separate the detonable mixture in the detonation section from the test gas in the driver section.

The nozzle expands the test gas from the stagnation condition in the driven section to hypersonic Mach numbers in the test section. The nozzle section is attached to the driven section by several coupled parts, through a locking mechanism which requires a 60^{o} rotation to secure the throat insert. This nozzle design permits interchangeable throat inserts, which allows for discrete test section Mach numbers ranging from 5 to 16. An interchangeable throat which results in the Mach 10 test section condition is currently used in the tunnel. The expansion nozzle is 101 inch long, with a 14^{o} conical expansion angle, and an exit diameter of 13.25 inch into the test section.

The test section houses the models used for the various experiments as quasi-steady hypersonic flow enters from the expansion nozzle exit. The test section is 21.1 inch long, and 17.5 inch in diameter. The test section is accessed by circular windows 9 inch in diameter, on

opposite sides of the tunnel. Transparent windows can be mounted on the circular ports, for flow visualization experiments, such as schlieren imaging. The exit of the test section converges, where it connects with the diffuser.

The diffuser section is a convergent section which reduces the flow Mach number as it proceeds to the dump tank. The diffuser section is 31.5 inch long, and converges from a diameter of 15 inch to 12.2 inch. Experimental models are mounted in the tunnel at the diffuser section and extend into the test section.

The dump tank terminates the hypersonic flow. The dump tank is attached to the diffuser outside the building, and has a volume of 150 ft^3. The dump tank has spring-loaded, pressure-sensitive safety valve, which is closed by vacuuming the dump tank, and opens due to excess pressure created as the flow stagnates, exposing the tunnel to atmospheric conditions.

2.1.1 Diaphragm Calibration

The primary diaphragm section uses gauge 10 hot-rolled steel sheets, which are 0.1196 inch thick. The steel diaphragms are pre-scored to a desired depth with a cross pattern shown in Figure 2.2. A CNC milling machine is the desired method for diaphragm scoring, because it ensures that the scoring depth is uniform within a diaphragm and consistent between diaphragms.

Figure 2.2 Primary diaphragms scored and after successful test

Diaphragm tests were performed to determine the ideal scoring depths for desired corresponding initial driver pressures. The diaphragm section is gradually filled to half the driver pressure till the desired initial driver pressure is reached. The optimal scoring depth is selected by ensuring that the diaphragm will not rupture during the filling process, and the diaphragm will rupture before the diaphragm section is completely vented. The results of the steel high pressure diaphragm calibration are listed in Table 2.1. Based on these results, diaphragms scored similar to test 2 depths, are used for tests when the initial driver pressure ranges from 200 atm to 300 atm, while diaphragms scored to similar test 3 depths are used when the initial driver pressure is greater than 300 atm.

Table 2.1 High-pressure diaphragm calibration

High-Pressure Diaphragm Test #	Scored Diaphragm Depth (inches)	Rupture Pressure (atm)
1	0.040	150
2	0.035	173
3	0.030	208

The detonation section is isolated from the driven section by a Mylar diaphragm. Preliminary testing of diaphragms was performed to ensure that the pre-detonation pressure of the detonable oxy-hydrogen mixture does not cause a rupture of the diaphragm during the filling process. The detonation section is gradually filled with air from the low pressure compressor, to determine the pressure at which the Mylar diaphragms rupture. The results of the Mylar diaphragm calibration are listed in Table 2.2. Mylar diaphragms of test 1 thickness are used for runs with pre-detonation pressures lower than 6 atm, while diaphragms with test 2 thicknesses are used for runs with pre-detonation pressures greater than or equal to 6 atm.

Table 2.2 Detonation section Mylar diaphragm calibration

Detonation Section Diaphragm Test #	Mylar Diaphragm Thickness (inches)	Rupture Pressure (atm)
1	0.010	6.8
2	0.020	>13.6

2.1.2 Tunnel Operation

The hypersonic shock tunnel can be operated in a low or high-enthalpy mode. Filling and venting of sections in the tunnel are controlled by pneumatic valves which are coupled to solenoid valves. The electrically-controlled solenoid valves allow low-pressure air from the low-pressure compressor to open or close the pneumatic valves.

The low-enthalpy mode is the basic operation mode of the tunnel, and requires a high-pressure gas in the driver, a low-pressure test gas in the driven section, and vacuum in the expansion nozzle, test section, diffuser and dump tank. The high-enthalpy mode employs a shock induced detonation driver. The high-enthalpy mode requires a high-pressure gas in the driver, a low-pressure detonable mixture in the detonation section, a low-pressure test gas in the driven section, and vacuum in the expansion nozzle, test section, diffuser and dump tank.

The high-pressure air in the driver is supplied from a system which comprises of a 5-stage compressor, a 2-stage booster pump and a spherical high pressure storage vessel. Air from the atmosphere is collected by the 5-stage compressor (Clark Model CMB-6), which provides dry compressed air with pressures up to 2100 psi. The high pressure air from the 5-stage compressor goes into the first booster pump (Haskel 55696) of the 2-stage booster, raising the pressure to 5000 psi. The air proceeds into the second booster pump (Haskel 55696) which compresses the air up to 9000 psi. The high-pressure air from the 2-stage booster pump is discharged into a one meter diameter spherical high-pressure storage vessel, which is rated for storage pressures up to 5500 psi.

Low-pressure air at 175 psi is supplied by a Kellogg American Inc. Model DB 462-C compressor pump. This low-pressure air is used by solenoid valves to control pneumatic valves

for the high-pressure, detonable gas, and vacuum pump system. This low pressure is reduced to 75 psi, to operate the 2-stage Haskel booster pump.

The detonable gas system comprises of a standard industrial oxygen and hydrogen tanks filled to 2000 psi. Pneumatic valves and pressure gauges are also incorporated into the system. The gas tanks are located outside the lab facility to alleviate safety concerns. Individual pneumatic valves for the fuel, vacuum, vent, air, oxygen, and transducer are used for controlled filling, venting, vacuuming and pressure monitoring of the detonation tube section. The pressure in the detonation section is monitored by a MKS Baratron pressure gauge; which has a maximum rating of 10000 mmHg.

The vacuum system comprises of two vacuum pumps for the driven, detonation, and test sections. The driven tube is evacuated by a Sargent-Welch Model 1376 vacuum pump; which has a free-displacement of 300 liters/min. The detonation section tubes are also evacuated using the same vacuum pump as for the driven section. The test section is separated from the driven section by a secondary Mylar diaphragm located in the nozzle throat. The test section is evacuated by a Sargent-Welch Model 1396 vacuum pump; which has a free-air displacement of 2800 liters/min. This high-volume vacuum pump is essential in evacuating the vast dump tank, in a timely manner. The pressure in the driven tube and the dump tank is measured by a MKS Baratron Type 127A pressure gauge; which has a maximum range of 1000 mmHg.

In preparation for a test, the driven section is first evacuated to 0.01 atm, and then filled with dry air from the low pressure compressor to 1 atm. The test section is evacuated to below 50 mbar, to ensure hypersonic flow starts in the nozzle. The detonation section is evacuated to 0.01 atm, filled first with hydrogen, and then filled with oxygen, to the desired stoichiometric oxy-hydrogen mixture at the chosen pre-detonation pressure using Dalton's law of partial pressures. The driver section is filled with high pressure air from the yellow sphere. The Haskell pump is turned on during the high pressure filling to accelerate the process and to reach the initial driver

pressure of 5000 psi. The double-diaphragm section pressure is maintained to half the driver pressure during the filling process.

The test is initiated by venting the intermediate pressure air from the double-diaphragm section, causing the high-pressure air in the driver to rupture the steel diaphragms. The pressure difference between the driver and the detonation tube generates a normal shock which propagates downstream into the detonation section. The normal shock initially creates a deflagration wave, which transitions into a detonation wave, only if the pre-detonation pressure is sufficiently high. The deflagration to detonation transition is more perceptible with low pre-detonation pressures $P_{100} < 2\ \mathrm{atm}$. The detonation wave ruptures the detonation section diaphragm, is partially reflected, and propagates a normal shock into the driven section. This normal shock is reflected by the secondary Mylar diaphragm and creates the test stagnation conditions, state 5. The air behind the reflected shock expands through the evacuated nozzle to hypersonic Mach numbers in the test section. The wave diagram for the reflected shock tunnel with a shock induced detonation driver is presented in Figure 2.3.

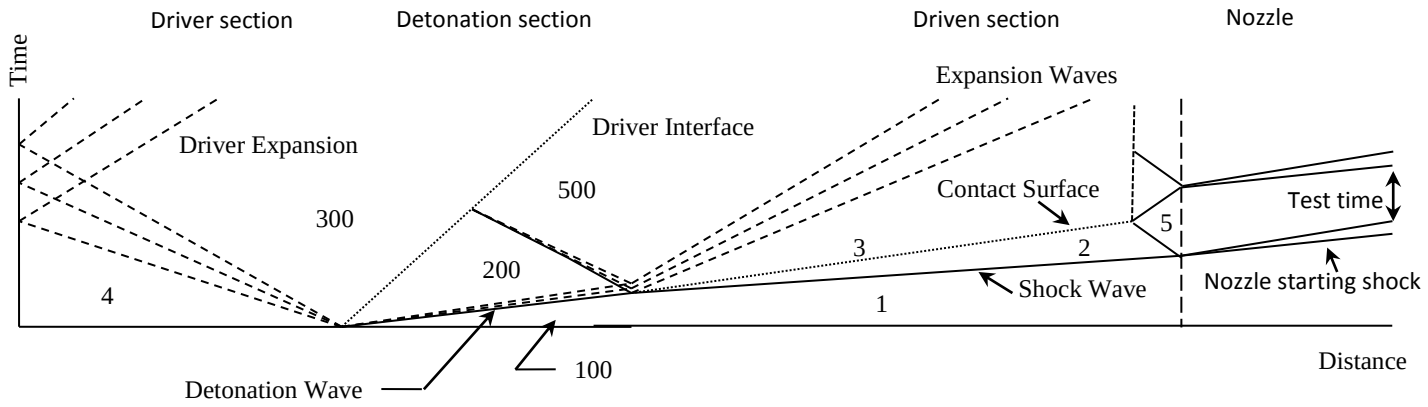

Figure 2.3 Wave diagram of shock induced detonation driver; adapted from Self [10].

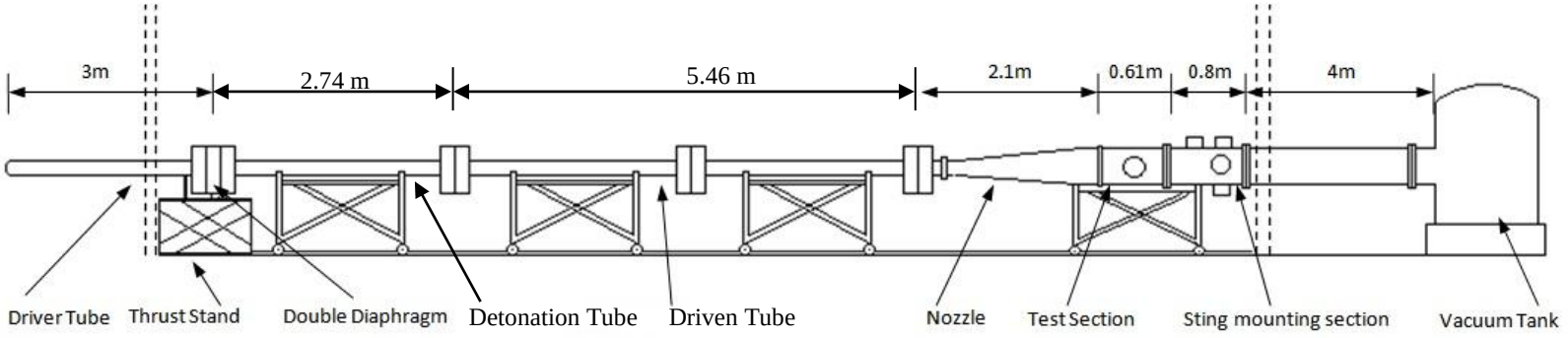

Figure 2.4 Schematic for UTA hypersonic shock tunnel; adapted from Vadassery [9].

2.2 Data Acquisition

Several transducers are used in this study, some mounted in ports on the shock tunnel, and at least one on the test model. Three high-pressure transducers (PCB 111A23) are mounted on each of the detonation and driven tube sections. These dynamic pressure transducers measure the conditions in the tunnel during operation. The position of the mounted PCB transducers along the detonation tube and driver tube sections is listed in Table 2.3. Using the time-of-flight method, wave propagation speeds can be deduced from the pressure outputs, and the distances between pressure transducers.

Table 2.3 Position of PCB transducer relative to distance from the double diaphragm.

PCB Transducer	Det 1	Det 2	Det 3	Pdet 1	Pdet 2	Pdet 3	Ch1	Ch2	Pt5
Position (in)	19.5	65.56	88.4	134.9	162.06	189.2	242.9	296.9	320.5

The output from the pressure transducers on the tunnel wall and in the test section is sent to a PCB model 483A signal conditioner. The output voltage is read by National Instruments TB-2709 data acquisition cards (NI-DAQs), and stored by a National Instruments PXIe-8130 embedded controller. Each DAQ card has 8 input channels, and by using 2 NI-DAQ cards, a maximum of 15 channels were available in this study. The DAQ is triggered by the signal corresponding to the incident shock measured via the p5 transducer, located furthest downstream on the driven tube. The DAQ is programmed via National Instruments LabVIEW software, to record data for 80 ms, with a 30 ms pre-trigger time, and at a sampling rate of 250 KHz/channel, for all channels.

2.3 Test section Experiments

The test section precedes the nozzle, which expands the test gas (air) from the driven section to hypersonic Mach numbers. The force balance and pressure rake experimental models are placed in the test section to characterize the performance of the shock tunnel, and the properties of flow in the test section. The characterization of the shock tunnel performance

is critical in creating flow properties desired for hypersonic models, such as ramjet and scramjet engines.

2.3.1 Force Balance and Model

Force balances are used to measure the aerodynamic forces, and moments generated by test models. An external force balance was designed using finite element analysis (FEA) principles, by Vadassery [9]. The force balance is designed with consideration of several constraints, such as size, strength of balance, model support attachment, sensor placement, ease of calibration, and machining simplicity.

The force balance and model must be accommodated in the test section which is 17.5 inch in length and 21.1 inch in diameter. The force balance is made from aluminium-606l because of it low density and high strength. The force balance is machined from a single block of aluminum 6061. Fabrication from a single block reduces stress concentration which is encountered if the beam members are fastened together. The force balance is 8.25 inch in length, 4.29 inch in height and 1 inch in width. The stress bars are angled 45^{o} from the model mount, and are 0.35 inch thick. Piezoelectric film strain gauges (Measurements Specialties Model DT1-052K) are mounted on angled stress bars, to measure the stress waves. Figure 2.5 shows a photograph of the fabricated force balance.

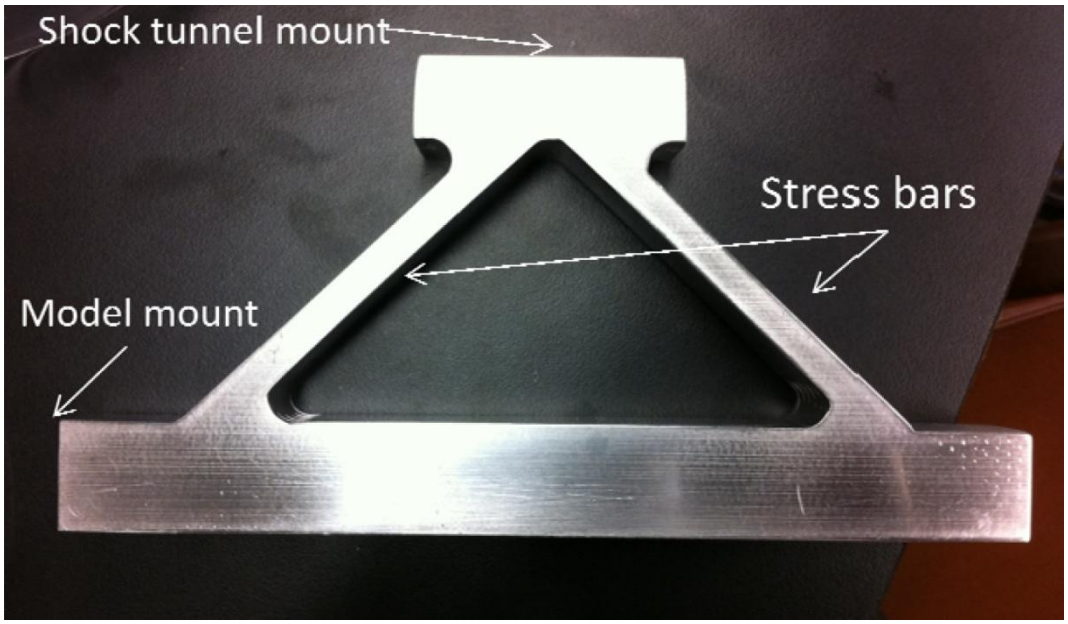

Figure 2.5 Force balance; Vadassery [9].

The force model is a blunt cone, used to validate the forces measured, by comparing them to predicted forces by Newtonian theory for a blunt cone. The model is made of steel, has a base radius of 1.575 inch, a length of 3.5 inch, and a half-angle of 18.5^{o}. The blunt cone model is designed to hold a PCB 111A21 pressure transducer mounted on its centerline. This pressure transducer measures the pitot pressure in the test section during the tests. Figure 2.6 shows a photograph of the fabricated blunt cone model.

Figure 2.6 Blunt cone force balance model; Vadassery [9].

The force balance is mounted to the top of the test section by two 0.5 inch diameter, 6 inch long, grade 9 steel bolts, 4.6 inches apart along the centerline of the shock tunnel. Rubber and steel washers coupled with steel nuts, are used in the bolt connections to ensure a vacuum tight seal on the test section mount. The force balance is mounted so that the blunt cone model is positioned in the core flow from the nozzle, since this contains the most uniform flow. Figure 2.7 shows the force balance and blunt cone model as mounted in the test section.

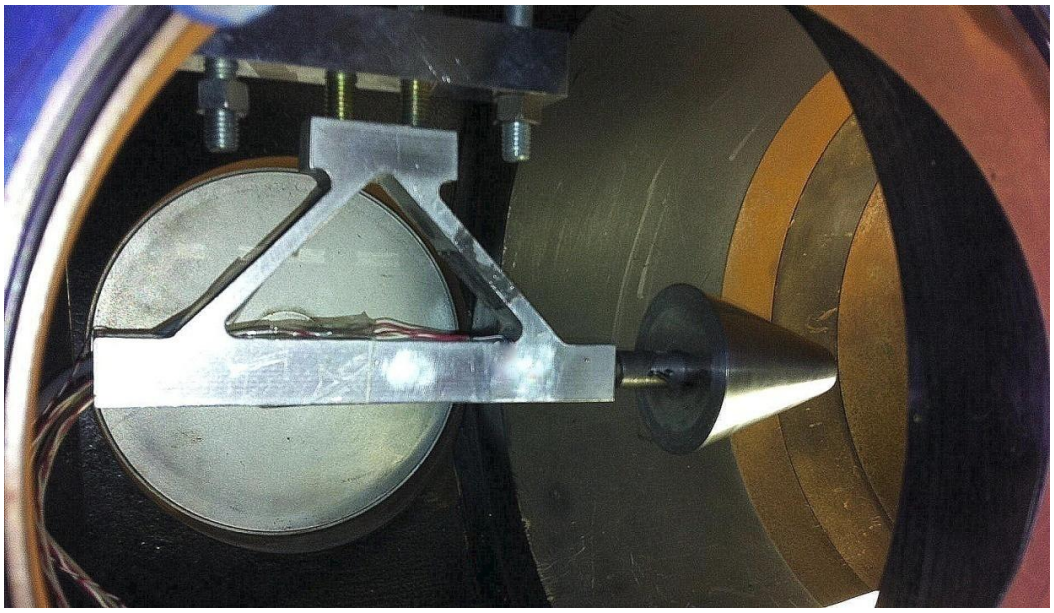

Figure 2.7 Force balance and model as mounted in test section; Vadassery [9].

2.3.2 Sting and Pressure Rake

A pressure survey of the test section is critical in determining the region in the test section which has uniform flow, and the characteristics of this core flow. In order to define the conditions of the flow, at least two state variables must be measured. Pressure and heat flux are measured simultaneously using a PCB 111A23 transducer and a Type K thermocouple, respectively. A sting and pressure rake with a hemispherical temperature port designed by Leamon, is used in this study [4]. The pressure rake was designed with consideration for several constraints, such as size, sensor placement, and machining simplicity.

Previous experimental runs of hypersonic shock tunnels have shown the boundary layer to be present in a minimum of 1/3 of the cross-sectional flow area from the nozzle. Therefore the pressure rake is designed to span two-thirds the length of the 13.25 inch nozzle exit diameter. This resulted in an 8 inch pressure rake facing the hypersonic flow. This length ensured that outermost pressure transducers are in the boundary layer. Nine PCB 111A24 pressure sensors are recess mounted on the pressure rake, equally spaced 1 inch apart, with the middle transducer positioned on the center-line axis of the test section.

The pressure rake and sting are made from aluminium-606l because of its low density and high strength. The leading edge of the rake is rounded and has a half angle of 3^{o}. This is the minimum angle which allows adequate area for the pressure transducers and wires in the cavity of the pressure rake. A bayonet style attachment with a hemispherical cap is positioned on the bottom of the rake along the center-line, and is used as the port for a Type K thermocouple. The leading edge of the pressure rake and the hemispherical cap are aligned on the same vertical plane, to prevent interference from the bow shock generated by each component.

The sting allows the rake to be precisely positioned along the centerline of the test section. The sting is mounted on the diffuser section by a 4 inch flange through which all the senor wirings from the pressure rake are channeled. The sting has a variable arm length design which allows for the rake to be positioned 4.64, 12.39, or 20.14 inch from the nozzle exit. The sting is positioned in the manner for which the leading edge of the rake is 12.39 inch from the nozzle exit for all high-enthalpy runs, Figure 2.8.

Figure 2.8 Sting and pressure rake as mounted in test section; Leamon [4].

CHAPTER 3

ANALYSIS AND RESULTS

The results of the characterization of UTA's Hypersonic Shock Tunnel are presented in this chapter, including discussion of the predicted performance of the hypersonic shock tunnel, the shock tunnel test conditions, detonation driver performance, and pitot pressure measurements.

3.1 Detonation Driven Shock Tunnel Analysis

The detonation shock tunnel analysis is initiated with the detonation tube section. The analysis used for the detonation driven shock tunnel is similar to that by Self [10]. The initial conditions, including the fuel-oxidizer ratio, and pre-detonation pressure, determine the post-detonation conditions, the post-reflected detonation conditions, and the ideal driver tube initial conditions. Using the fuel-oxidizer ratio, initial pre-detonation pressure (P_{100}), and the initial temperature (T_{100}), the NASA CEA online program is used to compute the burned gas, and detonation parameters via the 'det' option [11]. The burned gas and detonation parameter results are used to calculate the post-detonation wave properties which include: the burned gas pressure (p_{CJ}), the burned gas temperature (T_{CJ}), the burned gas density (ρ_{CJ}), the burned gas specific heat ratio (γ_{CJ}), the burned gas sonic velocity (a_{CJ}), the detonation wave Mach number (M_{det}), and the detonation wave velocity (u_{det}).

The NASA CEA online program does not calculate the post-reflected detonation gas conditions, region 500. The gas properties in this region are computed by a substitute solution using the NASA CEA burned gas conditions γ_{200}, $T_{200,}$ and assuming a calorically perfect gas. The calorically perfect gas sonic velocity equation is;

$$a_{200} = \sqrt{\gamma_{200} R T_{200}} \tag{3.1}$$

The post-reflected detonation wave Mach number is hence computed with;

$$\frac{M_{det,R}}{M_{det,R}^2-1} = \frac{M_{det}}{M_{det}^2-1} \sqrt{1+\frac{2(\gamma_{200}-1)}{(\gamma_{200}+1)^2}(M_{det}^2-1)(\gamma_{200}+\frac{1}{M_{det}^2})} \quad (3.2)$$

Using the reflected detonation wave Mach number, the post-reflected detonation gas conditions are calculated from the normal shockwave relations for a calorically perfect gas;

$$\frac{\rho_{500}}{\rho_{200}} = \frac{u_{500}}{u_{200}} = \frac{(\gamma_{200}+1)M_{200}^2}{2+(\gamma_{200}-1)M_{200}^2} \quad (3.3)$$

$$\frac{P_{500}}{P_{200}} = 1+\frac{2\gamma_{200}}{(\gamma_{200}+1)}(M_{200}^2-1) \quad (3.4)$$

$$\frac{T_{500}}{T_{200}} = \frac{h_{500}}{h_{200}} = \frac{2+(\gamma_{200}-1)M_{200}^2}{(\gamma_{200}+1)M_{200}^2} \left[1+\frac{2\gamma_{200}}{(\gamma_{200}+1)}(M_{200}^2-1\right. \quad (3.5)$$

The post-reflected detonation gas conditions, region 500, are characteristic of the overall performance of the detonation driver. The gas properties behind the incident detonation wave (region 200), are determined from the Chapman-Jouguet (CJ) detonation solution. In the perfectly-driven mode, the detonation tube burned gas pressure (P_{200}) matches the pressure of the expanded driver gas pressure (P_{300}). In the under-driven mode, the expanded driver gas pressure is less than the detonation tube burned gas pressure, hence Taylor rarefaction waves appear behind the incident detonation wave to match the expanded driver gas pressure boundary condition.

The initial conditions for the driver section can be computed from the information of the post-detonation Chapman-Jouguet detonation pressure. The driver tube gas is at a known temperature (T_4), pressure (P_4), and initially at rest (u_4=0). An iterative process is used to match the expanded driver gas tube pressure (P_{300}) to the burned gas tube pressure (P_{200}). The initial condition is equal velocities in the detonation tube section and the expanded driver tube section (u_{200}=u_{300}), and the solver iterates till the gas pressure in these regions match (P_{200}=P_{300}). The post-expansion wave driver gas properties are calculated from [12];

$$u_4+\frac{2a_4}{\gamma_4-1} = u_{300}+\frac{2a_{300}}{\gamma_4+1} \quad (3.6)$$

The initial driver gas section velocity is zero; hence, Equation 3.6 may be simplified in terms of the ratio of sound speeds;

$$\frac{a_{300}}{a_4} = 1 - \frac{\gamma_4 - 1}{2}\frac{u_{300}}{a_4} \tag{3.7}$$

The pressure, temperature and density are computed from the equations for the ratios across the expansion wave:

$$\frac{P_{300}}{P_4} = \left[1 - \frac{\gamma_4 - 1}{2}\frac{u_{300}}{a_4}\right]^{\frac{2\gamma_4}{\gamma_4 - 1}} \tag{3.8}$$

$$\frac{T_{300}}{T_4} = \left[1 - \frac{\gamma_4 - 1}{2}\frac{u_{300}}{a_4}\right]^2 \tag{3.9}$$

$$\frac{\rho_{300}}{\rho_4} = \left[1 - \frac{\gamma_4 - 1}{2}\frac{u_{300}}{a_4}\right]^{\frac{2}{\gamma_4 - 1}} \tag{3.10}$$

The analysis presented in Equations 3.6 to 3.10 accounts for the gas properties due to the expansion wave from the driver section. These properties of the gas in region 300 determine the characteristics of the gas behind the detonation wave which expands via Taylor rarefactions to match the velocity ($u_{300} = u_{200}$) across the slip line, referred to as the driver interface. The following equations describe the analysis of the gas properties behind the CJ detonation wave due to the presence of Taylor rarefaction waves;

$$u_{CJ} - \frac{2a_{CJ}}{\gamma_{CJ} - 1} = u_{200} - \frac{2a_{200}}{\gamma_{CJ} + 1} \tag{3.11}$$

where

$$u_{CJ} = u_{det} + a_{CJ} \tag{3.12}$$

and similarly Equation 3.11 solves for the ratio of the sound speed;

$$\frac{a_{200}}{a_{CJ}} = 1 + \frac{\gamma_{CJ} - 1}{2}\frac{u_{200} - u_{CJ}}{a_{CJ}} \tag{3.13}$$

The pressure, temperature, and density behind the CJ detonation are computed using:

$$\frac{P_{200}}{P_{CJ}} = \left[1 + \frac{\gamma_{CJ} - 1}{2}\frac{u_{200} - u_{CJ}}{a_{CJ}}\right]^{\frac{2\gamma_{CJ}}{\gamma_{CJ} - 1}} \tag{3.14}$$

$$\frac{T_{200}}{T_{CJ}} = \left[1 + \frac{\gamma_{CJ} - 1}{2}\frac{u_{200} - u_{CJ}}{a_{CJ}}\right]^2 \tag{3.15}$$

$$\frac{\rho_{200}}{\rho_{CJ}} = \left[1 + \frac{\gamma_{CJ} - 1}{2}\frac{u_{200} - u_{CJ}}{a_{CJ}}\right]^{\frac{2}{\gamma_{CJ} - 1}} \tag{3.16}$$

The computation of the velocity $u_{200}\,(u_{300})$ is iterated until the condition $P_{200} = P_{300}$ is matched. The iterated gas property solutions for region 200 are used in Equations 3.1 to 3.5 to solve for the post-reflected detonation gas wave properties; region 500.

The driven tube section is simulated using the NASA CEA online program, using the "shock" problem option. The analysis of the driver section and the detonation section resulting in a solution for the post-reflected detonation pressure P_{500}, and its ratio with the initial driven section pressure p1, is used to compute the Mach number of the incident shock wave in the driven section. This analysis is initiated by estimating a shockwave Mach number, then the corresponding the normal shock wave pressure ratio is computed for a calorically perfect gas using the following equation;

$$\frac{P_2}{P_1} = 1 + \frac{2\gamma_1}{(\gamma_1+1)}(M_s^2 - 1) \tag{3.17}$$

The resulting pressure ratio due to the incident normal shock is input into the following equation which results in the 'equivalent diaphragm' pressure ratio;

$$\frac{P_{500}}{P_1} = \frac{P_2}{P_1}\left[1 - \frac{(\gamma_{500}-1)(\frac{a_1}{a_{500}})(\frac{P_2}{P_1}-1)}{\sqrt{2\gamma_1[2\gamma_1+(\gamma_1+1)(\frac{P_2}{P_1}-1)]}}\right]^{\frac{-2\gamma_{500}}{\gamma_{500}-1}} \tag{3.18}$$

The incident shock wave Mach number is solved using a numerical method. This shockwave Mach number is input into the NASA CEA online program, selecting the "shock" problem option, and the reflected shock option. The program computes the gas properties behind the incident wave in region 2 $u_2,\ T_2,\ P_2,\ \rho_2,\ h_2$, and the reflected shock wave gas properties in region 5 $(u_5,\ T_5,\ P_5,\ \rho_5,\ h_5)$. The gas properties behind the reflected shock are the stagnation conditions for the flow through the nozzle and test section.

The maximum velocity the gas in the stagnation region can be expanded to through the nozzle is calculated using the hypersonic approximation;

$$h_5 + \frac{u_5^2}{2} = h_1 + \frac{V_{max}^2}{2} \tag{3.19}$$

$$V_{max} \cong \sqrt{2h_5} \tag{3.20}$$

Where u_5 is zero because the flow is stagnated, and the enthalpy h_1 is negligible; hence V_{max} in the test section is approximately a function of only the stagnation enthalpy.

3.1.1 Predicted Performance of HST with Detonation Driver

Using the analytical methods presented, the performance of the hypersonic shock tunnel is predicted using high-pressure air in the driver section, a stoichiometric oxy-hydrogen mixture in the detonation section, and low-pressure air in the driven tube. The initial driver pressure is 340 atm for all tests, and the initial temperature is 300 K for all tube sections, as shown in Table 3.1. The pre-detonation pressure is varied in in seven steps between a range of 1 and 8 atm. The driven section conditions are computed for an initial low air pressure at 0.1 atm and high air pressure at 1 atm. The results of the driven tube section are presented in Table 3.2. The stagnation enthalpy h_5 and the maximum velocity V_{max} are shown in Figures 3.1 and 3.2, respectively as a function of the pre-detonation pressure P_{100}. The stagnation enthalpy h_5 and pressure P_5 from the initial driven section pressure variation are presented in Figures 3.3 through 3.5.

Table 3.1 Initial conditions and computed performance map results for detonation and driver tube.

Detonation Tube Initial Conditions							
p_{100} (atm)	1.000	2.167	3.333	4.500	5.667	6.833	8.000
T_{100} (K)	300.	300.	300.	300.	300.	300.	300.
Detonation Tube Results							
u_{CJ} (m/s)	1293.2	1310.8	1320.5	1327.2	1332.4	1336.5	1339.9
p_{CJ} (bar)	18.904	42.136	65.607	89.555	113.71	137.8	162.24
ρ_{CJ} (kg/m^3)	0.89689	1.9443	2.9821	4.0284	5.0743	6.1111	7.1566
γ_{CJ}	1.1288	1.1330	1.1352	1.1367	1.1379	1.1388	1.1396
T_{CJ} (K)	3675.81	3825.35	3910.75	3971.88	4019.36	4057.93	4090.91
a_{CJ} (m/s)	1542.50	1566.90	1580.30	1589.70	1596.80	1602.50	1607.30
Driver Tube Initial Conditions							
γ_4	1.40	1.40	1.40	1.40	1.40	1.40	1.40
p_4 (atm)	340.00	340.00	340.00	340.00	340.00	340.00	340.00
T_4 (K)	300.	300.	300.	300.	300.	300.	300.
mol weight (kg/kmol)	28.97	28.97	28.97	28.97	28.97	28.97	28.97
a_4 (m/s)	347.2	347.2	347.2	347.2	347.2	347.2	347.2
ρ_4 (kg/m^3)	400.12	400.12	400.12	400.12	400.12	400.12	400.12
Driver Tube Results							
$u_{300} = u_{200}$ (m/s)	661.48	547.02	479.13	429.39	389.96	357.53	329.24
p_{300} (bar)	11.830	24.030	35.450	46.520	57.280	67.670	77.970
T_{300} (K)	114.93	140.72	157.25	169.94	180.36	189.15	196.97
a_{300} (m/s)	214.89	237.79	251.36	261.31	269.20	275.68	281.32
ρ_{300} (kg/m^3)	36.347	60.296	79.591	96.637	112.127	126.301	139.758
p_{200} (bar)	11.830	24.030	35.450	46.520	57.280	67.670	77.970
T_{200} (K)	3484.47	3581.37	3634.31	3671.16	3698.88	3721.14	3739.72
a_{200} (m/s)	1501.82	1516.11	1523.42	1528.33	1531.82	1534.56	1536.76
ρ_{200} (kg/m^3)	0.5922	1.1846	1.7339	2.2646	2.7777	3.2736	3.7625

Table 3.2 Initial conditions and computed performance map results for driven tube.

Low Pressure Driven Tube Initial Conditions							
p_1 (atm)	0.100	0.100	0.100	0.100	0.100	0.100	0.100
T_1 (K)	300.	300.	300.	300.	300.	300.	300.
mol weight (kg/kmol)	28.965	28.965	28.965	28.965	28.965	28.965	28.965
M_{shock}	7.6465	9.2974	10.2549	10.9415	11.4736	11.9044	12.2712
Low Pressure Driven Tube Results							
p_5 (bar)	62.24	109.03	143.17	169.39	190.07	206.74	220.84
T_5 (K)	4718.70	6240.81	7119.46	7653.89	8024.14	8302.26	8527.15
ρ_5 (kg/m^3)	4.2259	5.2023	5.7673	6.1691	6.4515	6.6520	6.8022
h_5 (kJ/kg)	7364.41	11060	13517.1	15385.3	16893.1	18151.9	19251.5
V_{max} (m/s)	3838	4704	5200	5548	5813	6026	6205
High Pressure Driven Tube Initial Conditions							
p_1 (atm)	1.000	1.000	1.000	1.000	1.000	1.000	1.000
T_1 (K)	300.	300.	300.	300.	300.	300.	300.
mol weight (kg/kmol)	28.965	28.965	28.965	28.965	28.965	28.965	28.965
M_{shock}	3.4863	4.5178	5.1675	5.6566	6.0490	6.3752	6.6589
High Pressure Driven Tube Results							
p_5 (bar)	81.03	161.86	228.34	286.84	339.42	387.26	432.18
T_5 (K)	1649.81	2452.72	2999.87	3418.61	3753.86	4031.84	4274.17
ρ_5 (kg/m^3)	17.1000	23.0000	26.5000	29.1000	31.2000	33.0000	34.5000
h_5 (kJ/kg)	1526	2592	3394	4065	4644	5155	5621
V_{max} (m/s)	1747	2277	2605	2851	3048	3211	3353

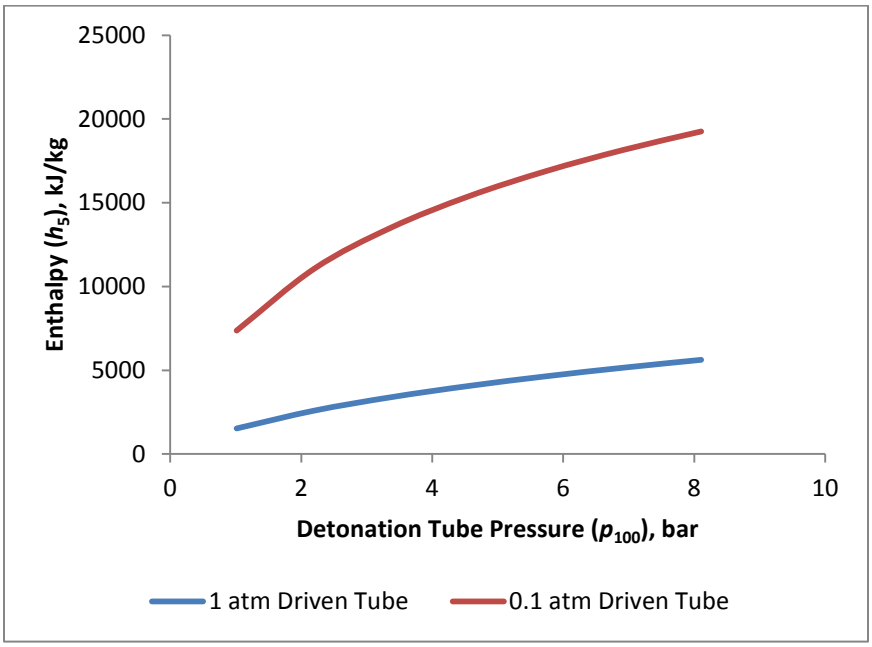

Figure 3.1 Predicted detonation tube enthalpy performance map.

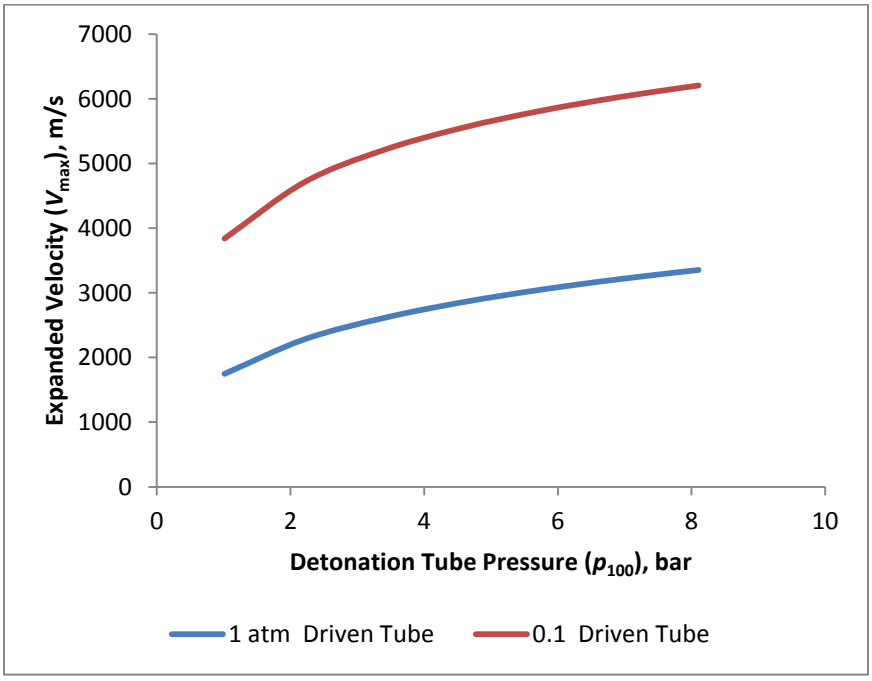

Figure 3.2 Predicted detonation tube expanded velocity performance map.

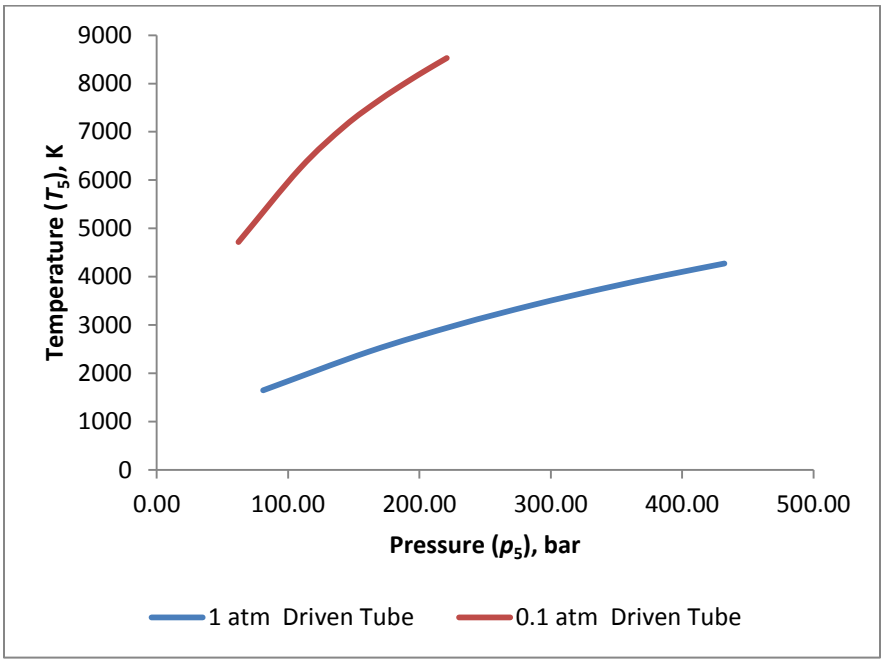

Figure 3.3 Predicted performance map of detonation-driven shock tube.

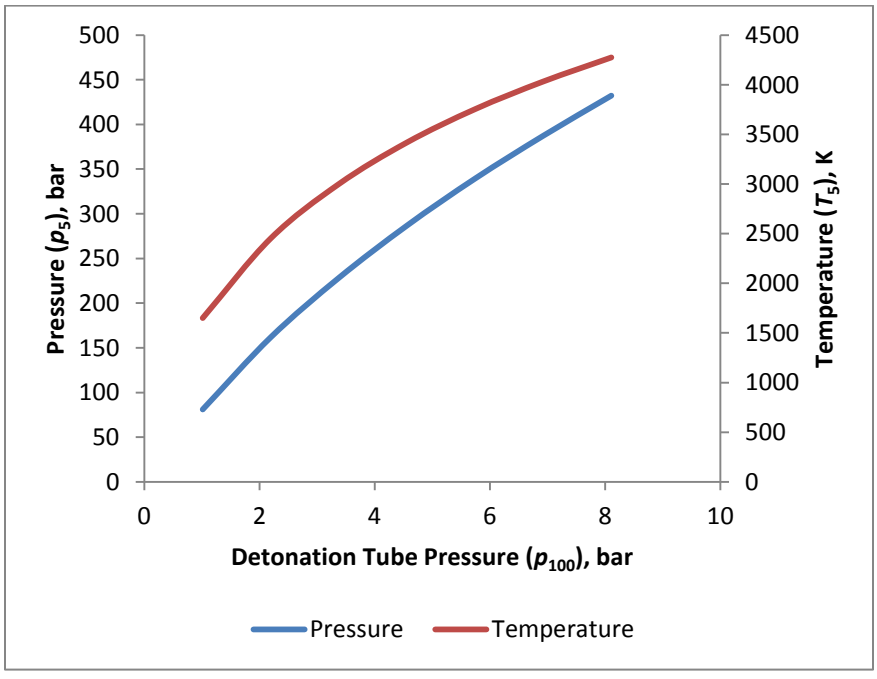

Figure 3.4 Variation of stagnation properties for 1 atm driven tube.

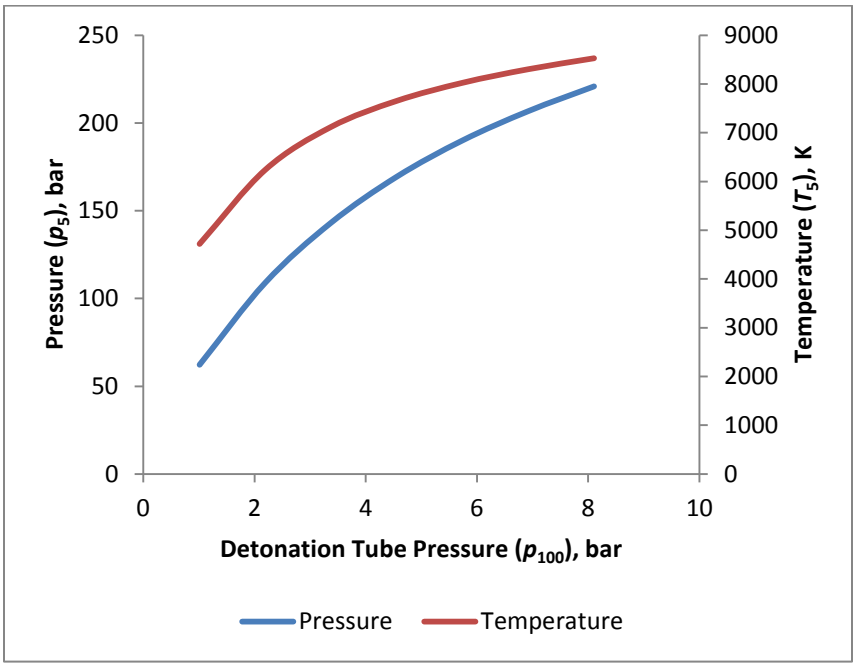

Figure 3.5 Variation of stagnation properties for 0.1 atm driven tube.

3.2 Test Methodology

In preparation for the high-enthalpy characterization of the UTA Hypersonic shock tunnel with a shock induced detonation driver, the following test plan was created. The primary considerations were variation of pre-detonation pressure, variation of detonation section volume, variation of driver pressure, and test repeatability. The initial pressure conditions of this study are listed in Table 3.3.

Table 3.3 High enthalpy characterization test plan

Single Tube Detonation Driver			
	Driver P_4(atm)	Detonation P_{100}(atm)	Driven P_1(atm)
Test #	Air	$2H_2+O_2$	Air
1	340	1	1
2	208	2	1

Table 3.3 - *Continued*

3	216	2	1
4	308	4	1
5	293	6	1
Double Tube Detonation Driver			
6	340	2	1
7	340	3	1
8	340	7	1

The variation of the pre-detonation pressure is limited to a maximum pressure of 8 atm in order not to compromise the structural integrity of the hypersonic shock tunnel, due to the significant rise of the post detonation pressure. The detonation section volume was varied from a single tube (1T) volume of 7.73 ft^3 to a double tube (2T) volume of 15.46 ft^3. The force balance was mounted in the test section for the 1T tests, while the pressure rake was mounted for the 2T tests. The driver section pressure is known to have a significant effect on the test time in the test section. The driver section pressure was varied from a minimum of 200 atm to ensure the shock is strong enough to induce the detonation wave, and limited to a maximum pressure of 340 atm in order not to compromise the structural integrity of the driver section. To ensure the repeatability of the detonation driver performance, the 2 atm pre-detonation test condition was repeated with similar initial driver and driven section conditions. The driven section pressure was not varied to simulate higher altitudes, because the primary focus of this study is increasing flow enthalpy, and matching conditions within the hypersonic air-breathing corridor.

3.2.1 Experimental Results

The experimental results of the shock-induced detonation driver performance are presented in this section. The pressure traces of the PCB transducers mounted along the detonation driver tube and the driven tube for the several tests performed with a detonation driver have similar characteristics; therefore, only the results from Test 1 in Table 3.2 are presented in Figures 3.1 to 3.6. In Figure 3.6, the pressure trace of 'det1' reflects the presence of a deflagration wave. The pressure transducers further downstream on the detonation tube show a high-pressure rise attributed to the detonation wave. Hence the deflagration-to-detonation transition occurs between pressure transducer 'det1' and 'det2.' The reflected detonation wave creates an incident shock in the driven tube shown by the pressure traces in Figure 3.7. The nozzle stagnation pressure measurement 'pt5' is also presented in Figure 3.7. The pressure transducer mounted in the force balance discussed in Chapter 2 measure the pitot pressure in the test section, Figure 3.8. This pressure measurement is essential in calculating the Mach number in the test section, and determining the time of uniform test gas flow.

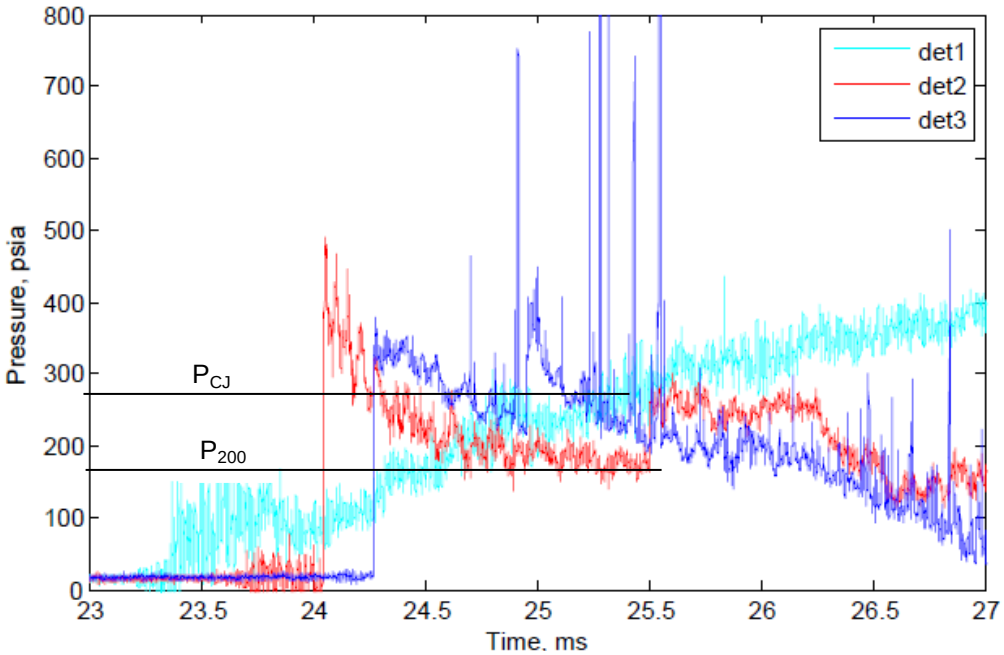

Figure 3.6 Detonation section tube pressure trace from Test 1.

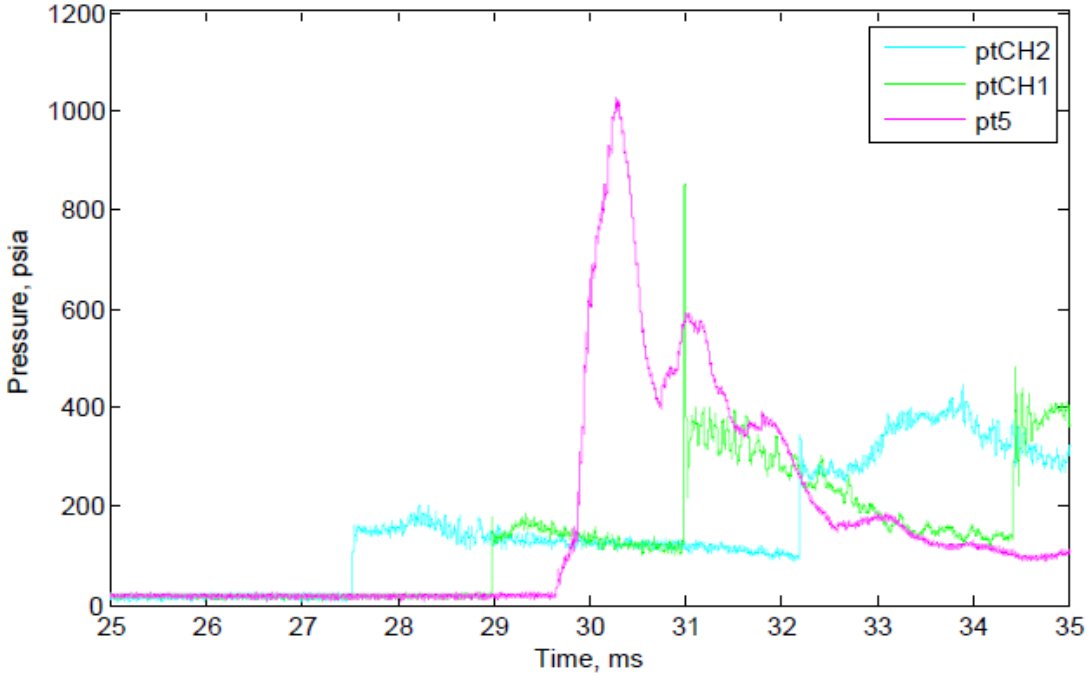

Figure 3.7 Driven section tube section pressure trace from Test 1

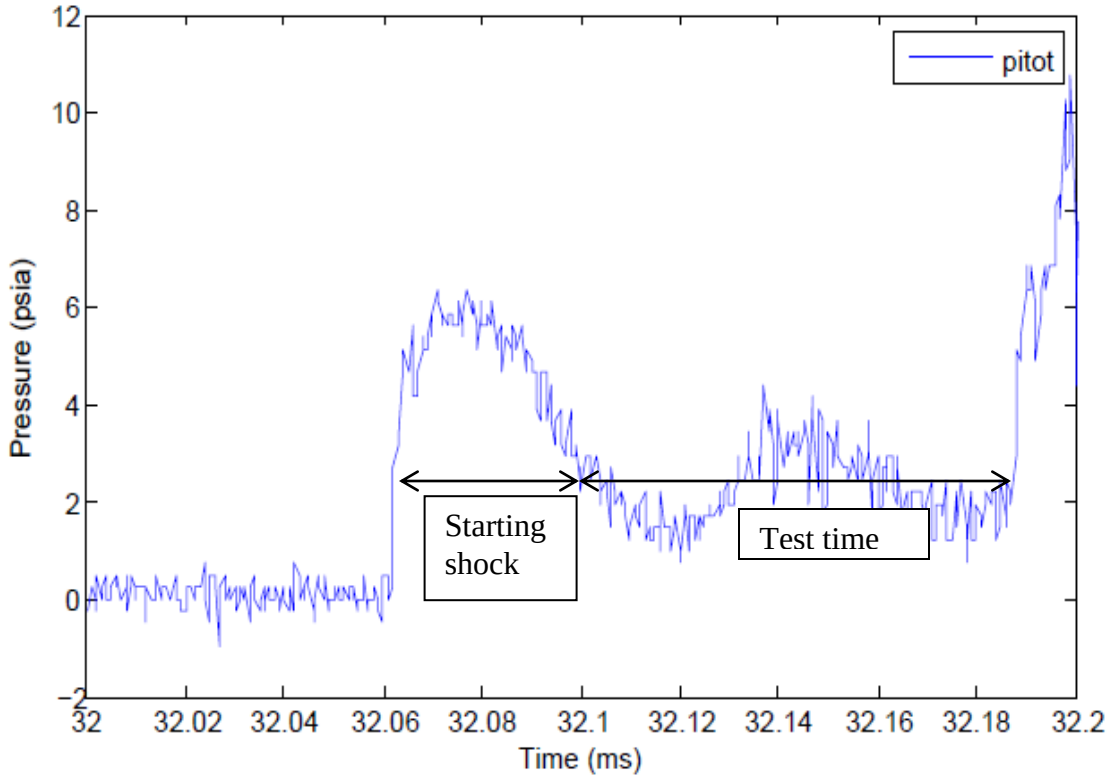

Figure 3.8 Test section pressure trace from Test 1.

The detonation and shock velocity for all the tests are calculated from the pressure trace measurements using the time-of-flight method. The measured velocities are recorded relative to the distance from the primary double diaphragm where each test is initiated. The results for the single detonation tube are presented in Figures 3.9 and 3.10. The legend "2atm3180" indicates a pre-detonation pressure of 2 atm and an initial driver pressure of 3180 psi. The results for the single detonation tube with 1 atm pre-detonation pressure are presented separately in Figure 3.10, due to velocity variation from the deflagration-to-detonation transition, not measured in subsequent tests with higher pre-detonation pressure. Figure 3.11 shows the incident shock wave velocity results for the double driven tube section tests. The results for the double detonation tube are presented in Figure 3.12, while Figure 3.13 shows the incident shock wave velocity results for the single driven tube section tests. The measured detonation wave speed is very close to the theoretical CJ detonation wave speed of 2.78 km/s for stoichiometric oxy-hydrogen. The deviations from this velocity are attributed to slight variation of the concentrations of the detonable gases due to minor leaks around the diaphragms. There is a significant decrease between the detonation wave speed and the incident shock velocity, primarily dependent on the initial pre-detonation pressure. The final shock velocities measured in the driven section are entered into the NASA CEA online program to solve for the gas properties behind the incident shock (region 2), and the gas properties behind the reflected shock (region 5).

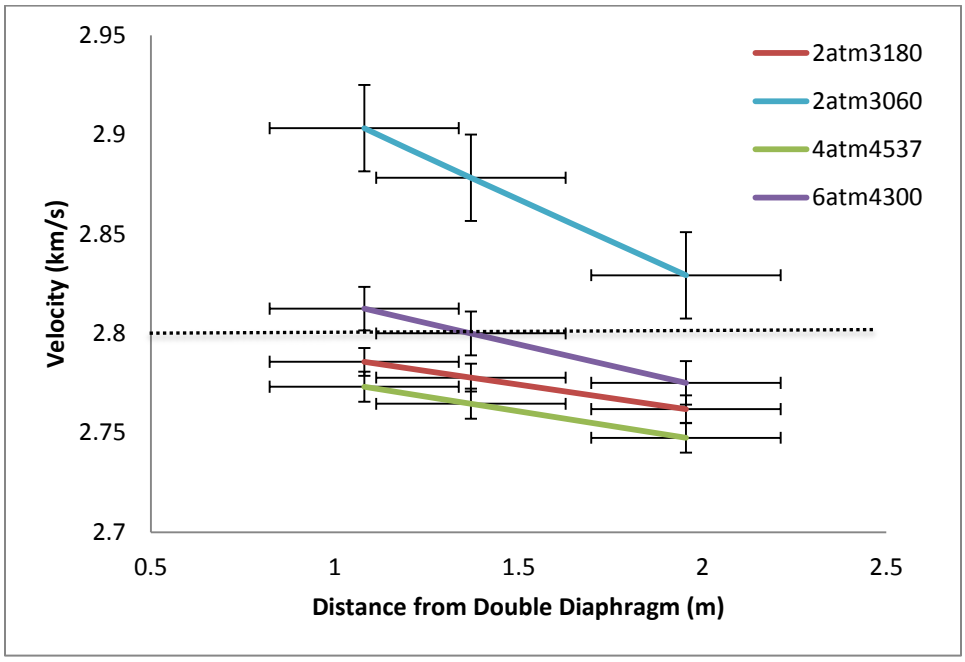

Figure 3.9 Single detonation tube section wave velocity

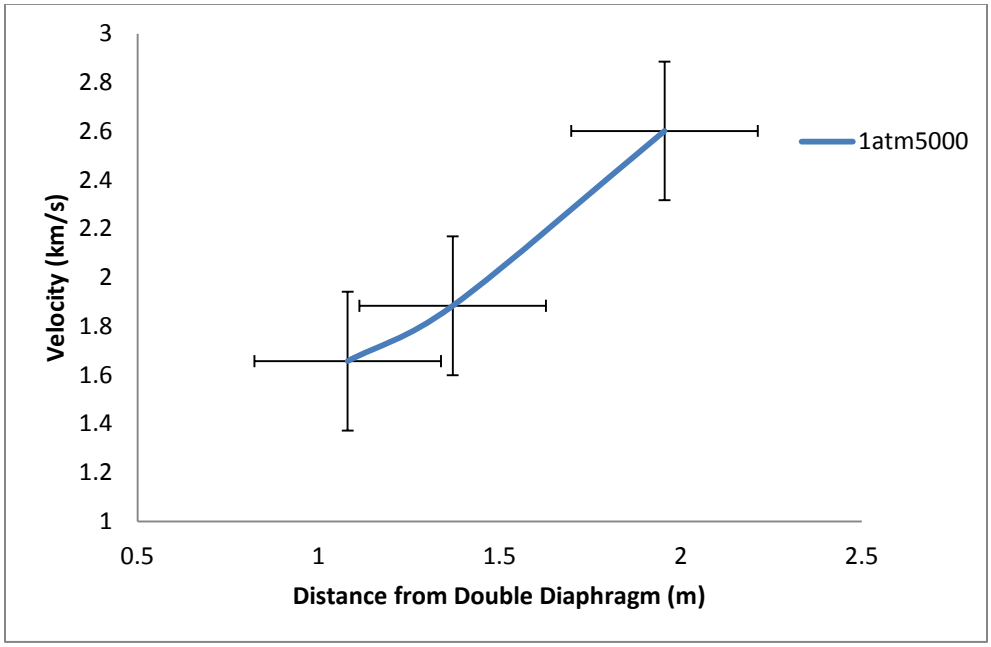

Figure 3.10 Single detonation tube section wave velocity for Test 1

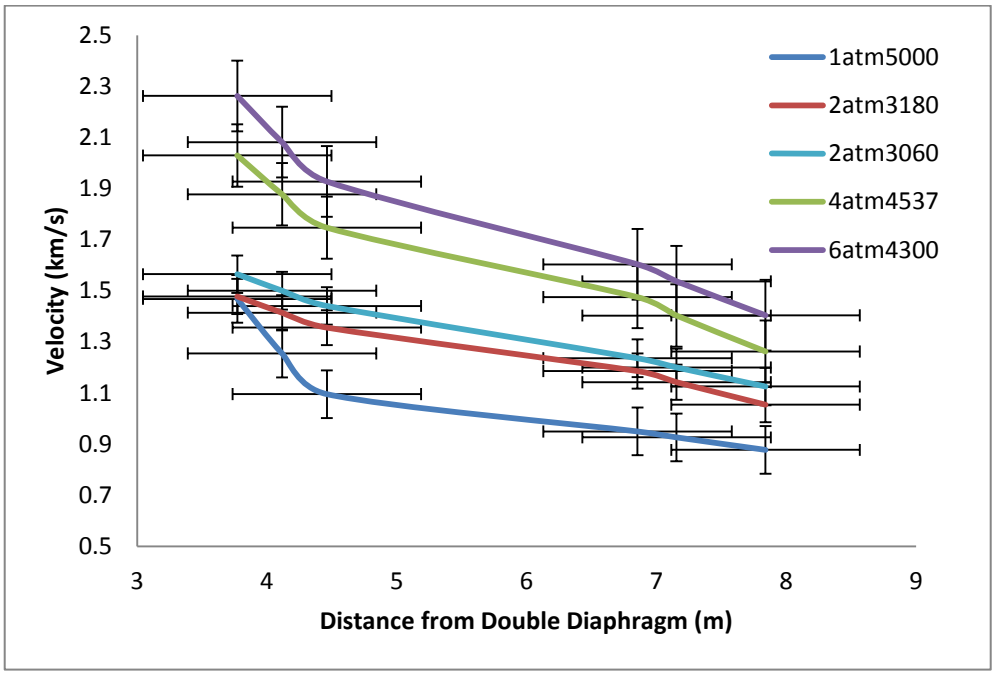

Figure 3.11 Double driven tube section shock velocity

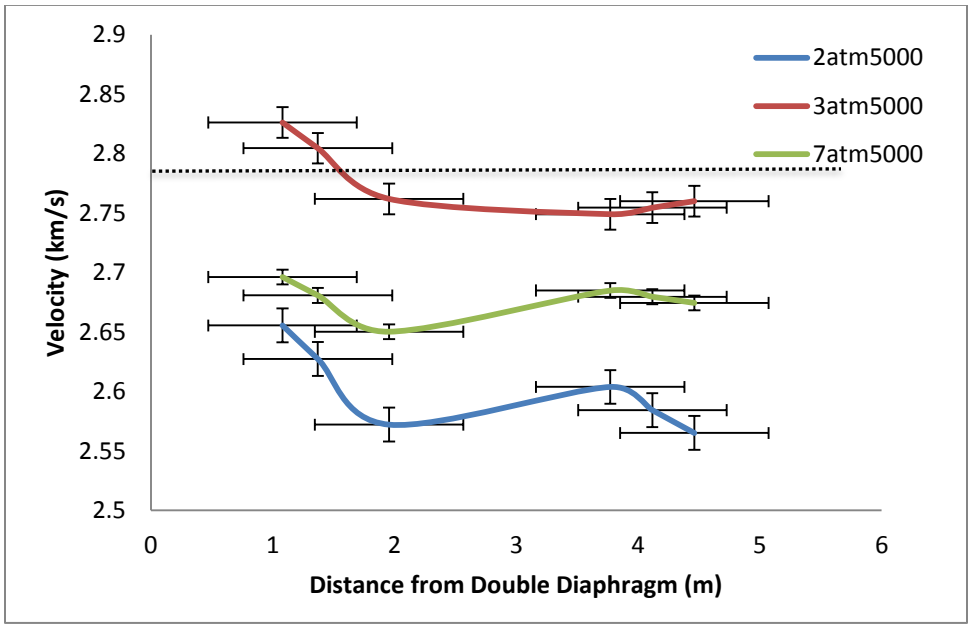

Figure 3.12 Double detonation tube section wave velocity

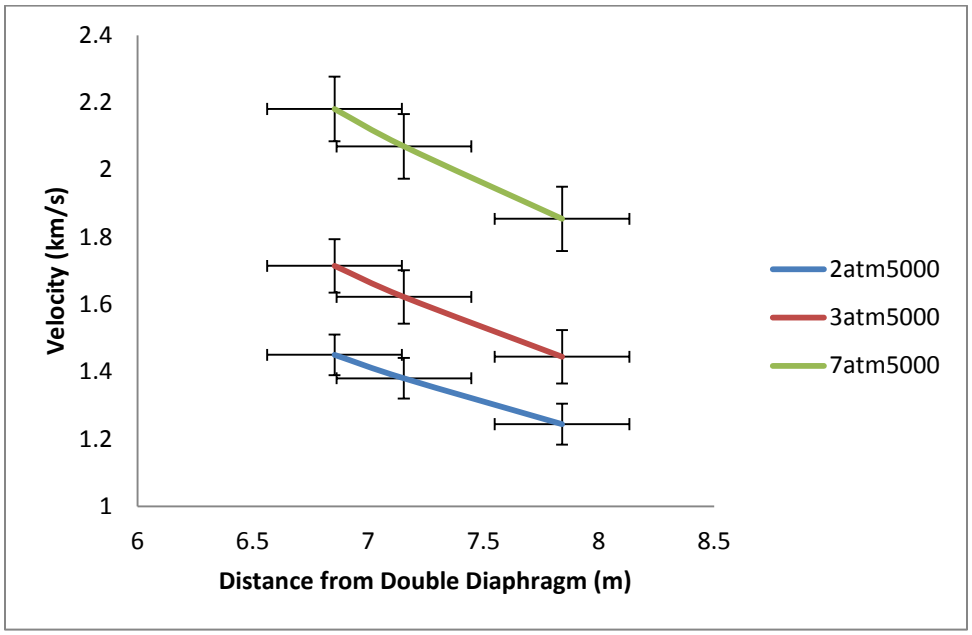

Figure 3.13 Single driven tube section shock velocity

The achievable stagnation enthalpy is a function of the pre-detonation pressure. Trend lines are added to graphs in Figure 3.14 to extrapolate the maximum achievable enthalpy with a pre-detonation pressure up to 8 atm, for the two detonation driver configurations. The stagnation pressure and stagnation temperature are shown in Figure 3.15. The experimental results for the stagnation section conditions are in close agreement with predicted values from earlier analysis for a high-pressure driven section. The stagnation pressure of 381 atm was calculated for the test 8, and is close to the maximum allowed pressure of 408 atm. The stagnation conditions of a low-enthalpy test are shown for comparison.

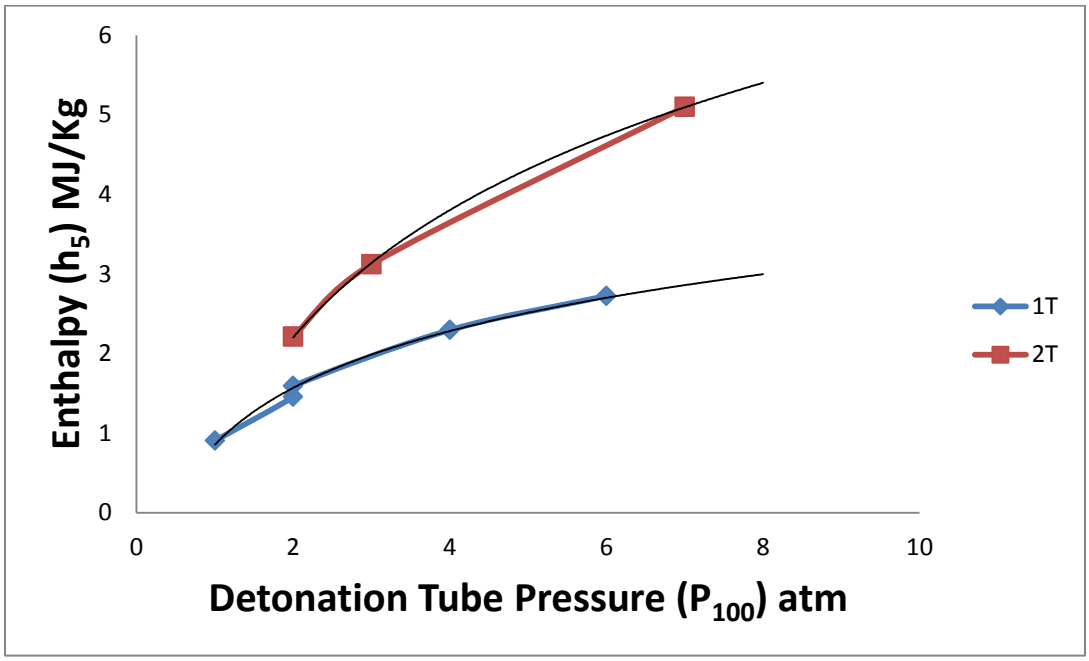

Figure 3.14 Stagnation enthalpy capability of detonation driver

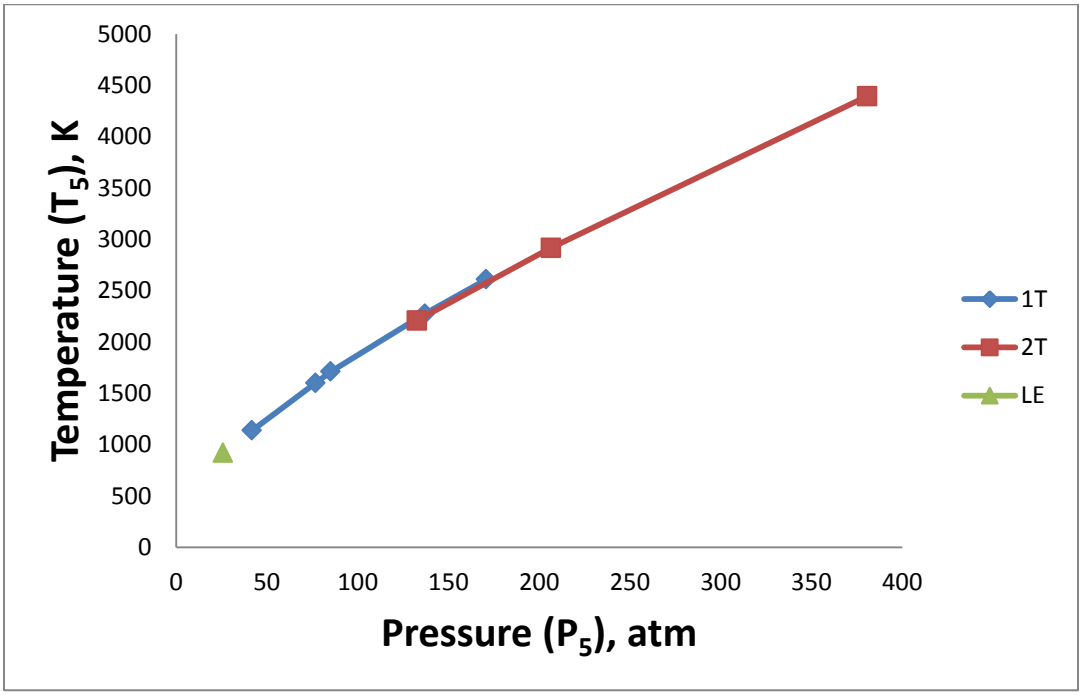

Figure 3.15 Performance map of UTA hypersonic shock tunnel

The Mach number in the test section is calculated using the isentropic relations for the ratio of the measured nozzle stagnation pressure (P_5) and the measured pitot pressure. Although the nozzle insert is designed for a nominal Mach number of 10, the average of the Mach number for the tests is 8.75, Figure 3.16. This decrease in Mach is attributed to the boundary layer within the nozzle. The minimal Mach number variation from different enthalpy tests indicate that the consistency of the performance of the hypersonic shock tunnel.

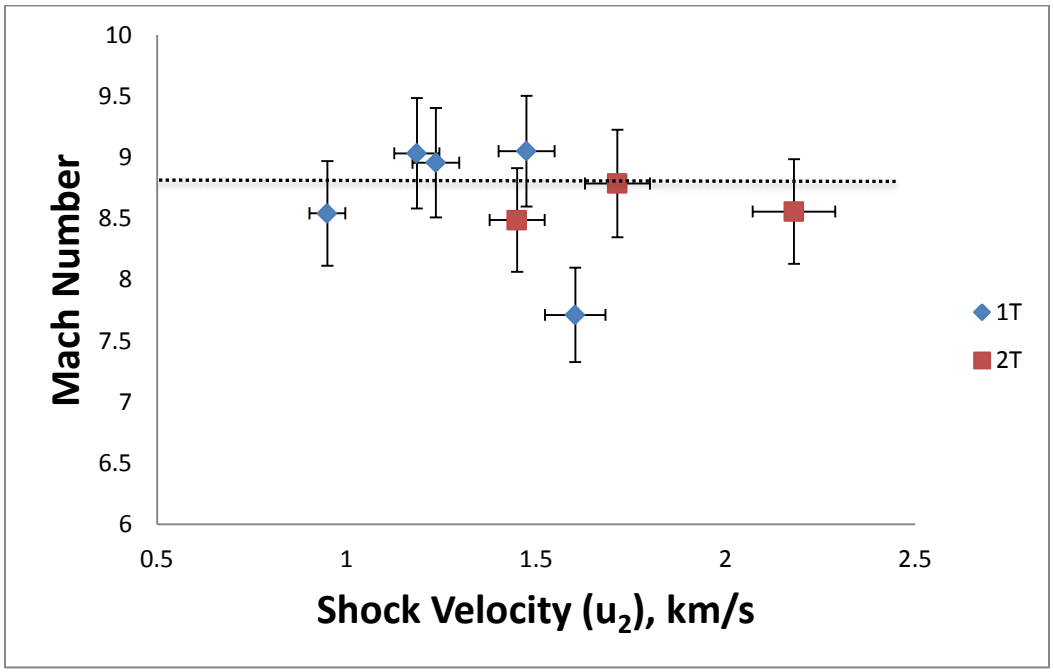

Figure 3.16 Test section Mach number variation

Multiple graphs of the various conditions within a tunnel are plotted to depict the performance of the tunnel. The most informative of these graphs is an altitude-velocity performance map. This graph shown in Figure 3.17 displays the hypersonic air-breathing corridor and highlights the region for which the UTA hypersonic shock tunnel experimental conditions are comparable for hypersonic flight.

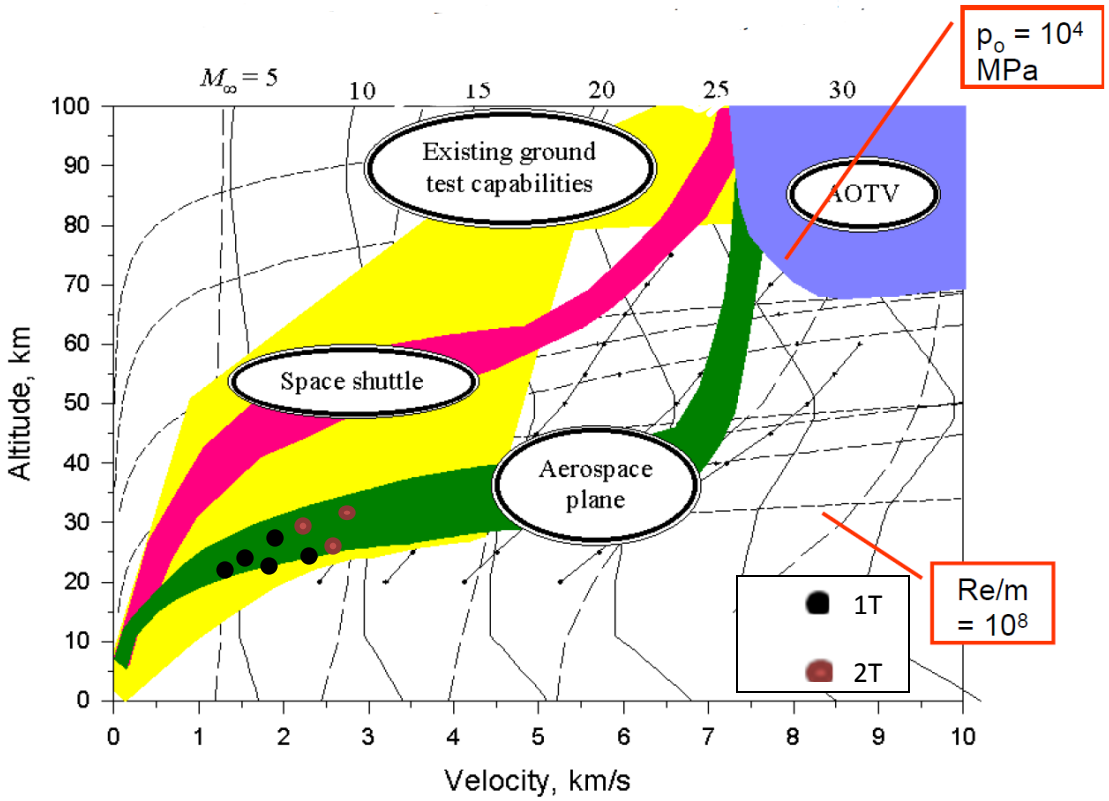

Figure 3.17 Detonation driver performance on hypersonic air breathing map; adapted from Lu [20].

CHAPTER 4

CONCLUSION AND FUTURE WORK

4.1 Conclusion

The performance of the UTA hypersonic shock tunnel is increased with the use of a shock induced detonation driver operated in the downstream mode. The pressure generated behind the detonation shock waves are measured using nine PCB dynamic transducers mounted along the detonation and driven tube sections respectively. The time-of-flight method is used calculate wave speeds between two transducers.

The detonation driver is powered with a stoichiometric oxy-hydrogen mixture. The detonable mixture is ignited by a strong shockwave created by high-pressure air from the driver section. The volume of the detonation driver is varied from a single tube to a double tube, to achieve the maximum possible flow enthalpy in the stagnation region. Experimental variation of the pre-detonation pressure is also performed, but the pressure of the detonable mixture is limited to 8atm in the double tube configuration, to ensure the stagnation pressure does not compromise the structural integrity of the hypersonic shock tunnel.

High-enthalpy flows with maximum total temperature of 4393 K, maximum total pressure of 373 atm, and maximum total enthalpy of 5.1 MJ/kg are achieved in the driven section, with a Mach number of 8.75 ± 0.25 measured in the test section.

4.2 Future work

To further improve the performance of the UTA hypersonic shock tunnel, tunnel improvement techniques discussed earlier may be implemented. A high-pressure helium gas driver, coupled with a free-piston-detonation driver, is capable of achieving significantly higher flow enthalpy in the stagnation region. An additional model with a static pressure probe may be

mounted in the test section allowing for two additional independent methods for calculating the test section Mach number; hence assuring the accuracy of the test section conditions.

The initial pressures of the driven section might be reduced to simulate higher altitudes in the performance map. Expansion nozzles with geometries for Mach numbers lower than 10; can be designed to simulate real gas effects at these conditions. Ionization gauges are being developed to measure the detonation and shock wave speeds with improved resolution; using the time of flight method with ionization gauges mounted a few millimeters apart on the detonation tube.

.

APPENDIX A

DETONATION RUN PREPARATIONS

All Diaphragms have been placed as shown in the figure, and the yellow sphere is filled to 4500psi. Instructions 2-5 should be completed in the control room, with the wind tunnel room evacuated.

First Test:

Region 4 and 1 are filled with air, while region 100 is filled with the detonation mixture.

P4 = 3500 psi P100=30 psi P1=15 psi T4 = T100 = T1 = 300 K

Detonation gases : $2H_2+O_2 \rightarrow 2H_2O$ P_{H2}:P_{O2}, 2: 1 $\frac{P_{H_2}}{P_{Mix}} = \frac{2}{3} = \chi_{H_2}$ $\frac{P_{O_2}}{P_{Mix}} = \frac{1}{3} = \chi_{O_2}$

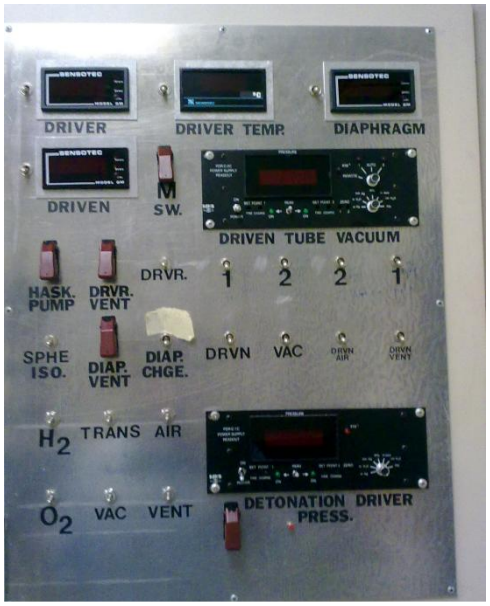

Figure A.1 Picture of control panel for UTA hypersonic shock tunnel.

1. Vacuum the test section, driven gas section tube, and detonation section tube.
    a. Open vacuum pump valve on the driven section
    b. Open 175 Air valve on the driven section.
    c. Turn on the test section and driven section vacuum pump.
    d. In control room, Turn on main switch.
    e. Monitor test section and driven section pressures.
    f. To vacuum detonation section, turn on detonation section display.
    g. Flip “trans” (transducer) switch to the on position.

h. Next flip the “vac” (detonation section vacuum) switch on.

i. Continue vacuuming till desired vacuum pressure is reached (<.02atm=.3psi).

j. Flip the “vac” (detonation section vacuum) switch OFF.

k. CLOSE vacuum pump valve on the driven section.

l. CLOSE vacuum pump valve for the Test section

m. Turn OFF driven section vacuum pump.

n. Turn OFF test section vacuum pump.

o. Record Driven, Test section, and Detonation section vacuum pressures from control room displays.

2. Fill driven section with air from the control room.

   a. Display driven section pressure.

   b. Flip “Drvn Air” switch to the on position and monitor transducer display.

   c. Flip “Drvn Air” switch to the OFF position when desired Driven section pressure is reached (~1atm=14.7psi)

3. Fill detonation section with fuel (H_2) first, followed by the oxidizer (O_2) in correct stoichiometric ratio (H_2:O_2, 1.11: 8.89). $2H_2+O_2 \rightarrow 2H_2O$

   a. In Control room, flip “trans” (transducer) switch to the on position.

   b. Monitor the detonation pressure display closely.

   c. The corresponding pressure ratios can be found using the Ideal gas law; P=nRT/V, where n is the moles of the substance, and Dalton’s law of partial pressures $P_{total} = P_{H2} + P_{O2}$. ($P_{H2}$:$P_{O2}$, 2: 1).

   d. Flip “H2” (fuel) switch to the on position.

   e. Fill to desired pressure as determined from stoichiometric ratio (~20psi).

   f. Flip “H2” (fuel) switch to the OFF position. Record the detonation pressure display

g. Flip “O2” (oxygen) switch to the on position.

h. Fill to desired pressure as determined from stoichiometric ratio (~30psi).

i. Flip “O2” (oxygen) switch to the OFF position. Record the detonation pressure display

j. Wait 15 minutes for fuel and oxidizer to diffuse within the tube.

k. Should any problems arise, vent the detonation section, by flipping the “vent” switch to the on position.

4. Fill diaphragm section with 1500 psi of air, and the driver section with 3000 psi of air.

    a. Flip the “Sphe Iso” switch to the on position.

    b. During the fill process monitor that the Diaphragm pressure is half the driver pressure.

    c. Flip “Drvr” switch to the on position and monitor “Driver” transducer.

    d. Flip “Diap chag” switch to the on position and monitor “Diaphragm” transducer.

    e. Flip “Drvr” switch to the OFF position.

    f. Flip the “Sphe Iso” switch to the OFF position.

    g. Fill driver till desired driver pressure is achieved (~3500 psi).

5. Vent diaphragm section to rupture the double diaphragms, and create shock induced Detonation.

    a. Record pressure transducer final readings. “Diaphragm”, “Driver”, “Driven temp.” and “Detonation section”

    b. Flip “trans” (transducer) switch to the OFF position.

    c. All filling and venting switches should be in the OFF position.

    d. Flip the “Diap vent” switch to the on position.

    e. Ruptures the double diaphragms, and creates shock induced Detonation.

6. After Test

    a. Purge the tunnel

b. Open sphere driver for 1min to allow reactants out.

APPENDIX B

MATLAB® PROGRAM

Similar MATLAB® programs to the one below is used in the analysis of all the experimental test results.

```
clc;
clear;
load D1atm.mat
y=D1atm;          x=y(:,1)*10^3;
% Pcb model 111A23 transducers max-100psi sensitivity- 50mv/psi(+-  10mv/psi)
pt4=y(:,2)*2000+14.7;       pdet3=y(:,8)*2000+14.7;
det1=y(:,3)*2000+14.7;      ch2=y(:,9)*2000+14.7;
det2=y(:,6)*2000+14.7;      ch1=y(:,10)*2000+14.7;
det3=y(:,5)*2000+14.7;      pt5=y(:,11)*2000+14.7;
pdet1=y(:,4)*2000+14.7;     pitot=y(:,12)*200;
pdet2=y(:,7)*2000+14.7;


P2=mean(pt5(74575:74700))
Ppit =mean(pitot(80125:80475))


ptest= y(:,12)*200;
figure (5)
plot(x,pt5,'c', x,ptest,'g');
hold on
[B,A] = butter(1,.002,'low');
Ytest = filter(B,A,ptest);
plot(x,Ytest,'b');
hold on
[B,A] = butter(1,.02,'low');
```

```
Ypt5 = filter(B,A,pt5);
plot(x,Ypt5,'b');

%% Test Section Transducers
figure (7)
plot(x,pitot,'b');
xlabel('Time (ms)')
ylabel('Pressure (psia)')
title('Test Section Pressure Trace')
legend('pitot')

figure (1)
plot(x,pt4,'c', x,det1,'g', x,det1,'b',  x,det2,'b',x,det3,'r', x,pdet1,'m', x,pdet2,'y', x,pdet3,'k',
x,ch2,'y-', x,ch1,'r-',x,pt5,'g-')
hold on;
xlabel('Time (ms)')
ylabel('Pressure (psia)')
title('Pressure vs. Time')
legend('pt4','det1','det2','det3','pdet1','pdet2','pdet3','ch2','ch1','pt5')

%% Driven Section
%% Detonation Tube section
figure (2)
plot(x,det1,'c', x,det2,'r',x,det3,'b')
hold on;
xlabel('Time (ms)')
```

```
ylabel('Pressure (psia)')
title('Pressure vs. Time in the Detonation Tube Section')
legend('det1','det2','det3')

ddet1det2=1.75-.58; ddet2det3=.58;  ddet1det3=1.75;
tsdet1=.02334; tsdet2=.024046; tsdet3=.024269;
udet1det2=ddet1det2/(tsdet2-tsdet1) % 1.6572*10^3 ??
udet2det3=ddet2det3/(tsdet3-tsdet2) %2.6009*10^3
udet1det3=ddet1det3/(tsdet3-tsdet1) %1.8837*10^3 ??

%% post detonation
figure (6)
plot( x,pdet1,'g',x,pdet2,'r',x,pdet3,'b')
hold on;
xlabel('Time (ms)')
ylabel('Pressure (psia)')
title('Pressure vs. Time in the Post Detonation Tube Section')
legend('pdet1','pdet2','pdet3')
dpdet1pdet3=1.38; dpdet1pdet2=.69; dpdet2pdet3=.69;
tspdet1=0.02515; tspdet2=.02562; tspdet3=.02625;
updet1pdet2=dpdet1pdet2/(tspdet2-tspdet1) %1.4681*10^3
updet2pdet3=dpdet2pdet3/(tspdet3-tspdet2) %1.0952*10^3
updet1pdet3=dpdet1pdet3/(tspdet3-tspdet1) %1.2545*10^3

%% stagnation tube section
```

```
figure (3)
plot(x,ch2,'c', x,ch1,'g',x,pt5,'m')
hold on;
xlabel('Time (ms)')
ylabel('Pressure (psia)')
title('Pressure Trace in the Stagnation Tube Section')
legend('ptCH2','ptCH1','pt5')
dch1ch2=1.3716; dch1pt5=.55; dch2pt5=1.3716+.55;
tsch2=.027538;    tsch1=.028983;     tspt5=.029668;
uch1ch2=dch1ch2/(tsch1-tsch2) %949.2042
uch1pt5=dch1pt5/(tspt5-tsch1)   %802.9197
uch2pt5=dch2pt5/(tspt5-tsch2)   %902.1596

% Driven section
figure (4)
plot( x,pdet2,'g', x,pdet3,'b', x,ch1,'r', x,ch2,'k',x,pt5,'m')
hold on;
xlabel('Time (ms)')
ylabel('Pressure (psia)')
title('Pressure vs. Time in Driven Section')
legend('ptd1','ptd2','ptd3','ptCH1','ptCH2
```

REFERENCES

1. Warren WR, Harris CJ " A critique of high performance shock tube driving techniques. Shock Tubes. Proc 7th Int Shock Tube Symp., June 23-25,1969ed. By I.I Glass, Univ Toronto Press, 143-176.

2. Coates, P.B., Gaydon, A.G., (1965) 'A simple shock tube with Detonation Driver Gas.' Proc. Roy. Soc. A 283:18-m3, 1964.

3. Bird, G.A, "A note on combustion driven shock tubes." AGARD Rep 146. B-VII, 1957.

4. Leamon, G. Derek, "Characterization of UTA Hypersonic Shock Tunnel," Master's Thesis, Department of Aerospace Engineering, The University of Texas at Arlington, Arlington, TX, 2012.

5. Lu, F.K. and Wilson, D.R., "Detonation driver for enhancing shock tube performance," Shock Waves (2003) 12:457-468

6. Hertzberg, A., et al. "Development of the Shock Tunnel and its Application to Hypersonic Flight," Progress in Astronautics and Rocketry, Volume 7, 701 (1962).

7. Stalker RJ "A study of free-piston shock tunnel." AIAA J 5(12): 2160-2165

8. Stuessy, W. Scott, "Hypersonic Shock Tunnel Development and Calibration," Master's Thesis, Department of Aerospace Engineering, The University of Texas at Arlington, Arlington, TX, 1989.

9. Vadassery, Pravin, “Design, Calibration and testing of a force balance for a hypersonic shock tunnel,” Master's Thesis, Department of Aerospace Engineering, The University of Texas at Arlington, Arlington, TX, 2012.

10. Self, Jason, “Performance of a Hypersonic Detonation Driver,” Master's Thesis, Department of Aerospace Engineering, The University of Texas at Arlington, Arlington, TX, 2011.

11. CEARUN. Ed. Dr. Michael J. Zehe. NASA. 22 Mar. 2012 <http://cearun.grc.nasa.gov/>

12. Anderson, John D., Jr.: *Modern Compressible Flow: With Historical Perspective,* 3d ed., McGraw-Hill Book Company, New York, 2003.

13. Zucrow Maurice J., Hoffman Joe D., “ Gas Dynamics” volume 1, John Wiley & Sons, Inc.,1976.

14. Heiser, W.H. and Pratt, D.T., *Hypersonic Airbreathing Propulsion*, AIAA Education Series, Washington D.C., 1994.

15. Anderson, John D., Jr., *Fundamentals of Aerodynamics*, 4th ed., McGraw-Hill, New York, 2007.

16. Stuessy, W.S., Murtugudde, R.G., Lu, F.K. and Wilson, D.R., "Development of the UTA Hypersonic Shock Tunnel," Paper 90-0080, AIAA 28th Aerospace Sciences Meeting, January 8-11, Reno, Nevada, 1990.

17. Zhao, w., Jiang, Z.L, Saito, T., et al, "Performance of a detonation driven shock tunnel," Shock Waves; Digital Object Identifier (DOI) 10.1007/s00193-004-0238-1, 2004.

18. Yu, Hu-r., Esser B., et al, “Gaseous detonation driver for a shock tunnel," Shock Waves 2:245-254, 1992.

19. Mirels, H., “Attenuation in Shock Tube due to Unsteady-Boundary Layer Action,” NAXCA Report 1333 1957.

20. Lu, F.K. "AE 5301-004 Hypersonic Wind Tunnel Techniques Notes," (2011).

BIOGRAPHICAL INFORMATION

Raheem Bello was born in Nigeria, on the 21st of October, 1992. He was inspired to study Astronomy from gazing at the night sky, and aspired to become an astronaut. In February 2006, he moved to the U.S. and resumed at Westbury high school in the 9th grade. He later graduated in spring 2008, and resumed college at University of Texas at Austin. At UT Austin, He worked in the Magnetism and Superconductivity group for 2 years studying “Thermal conductivity due to magnon heat transport.” He graduated from UT Austin in spring 2012 with a Bachelor of Science in Astronomy and a Bachelor of Science in Physics with honors. He enrolled at University of Texas at Arlington in Fall 2012, and resumed research at the Aerodynamics Research Center (ARC). He hopes to continue working at the ARC, while pursuing a doctorate degree in Aerospace engineering.